X-rays constraints on sub-GeV dark matter

Based on work with Cirelli, Fornengo, Pinetti & Roach 2303.08854

Jordan Koechler
LPTHE, Sorbonne University, Paris

Rencontres de Blois 2023

Introduction

Introduction

- No WIMP signals observed in collider searches, direct and indirect detection…

Introduction

- No WIMP signals observed in collider searches, direct and indirect detection…

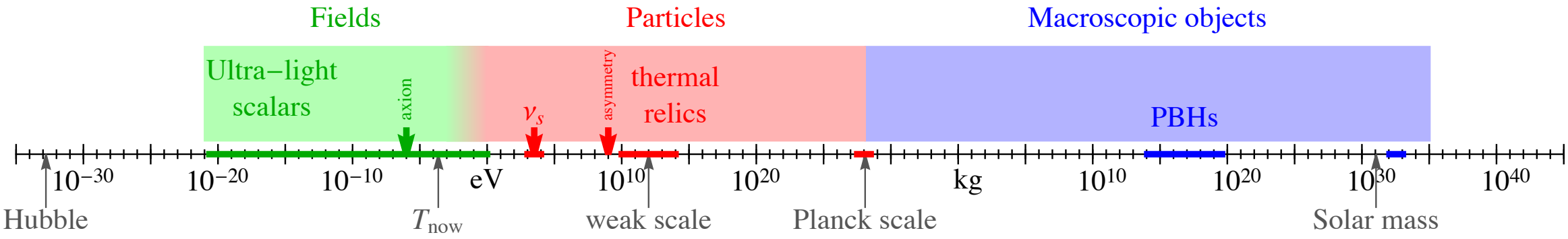

Introduction

- No WIMP signals observed in collider searches, direct and indirect detection…

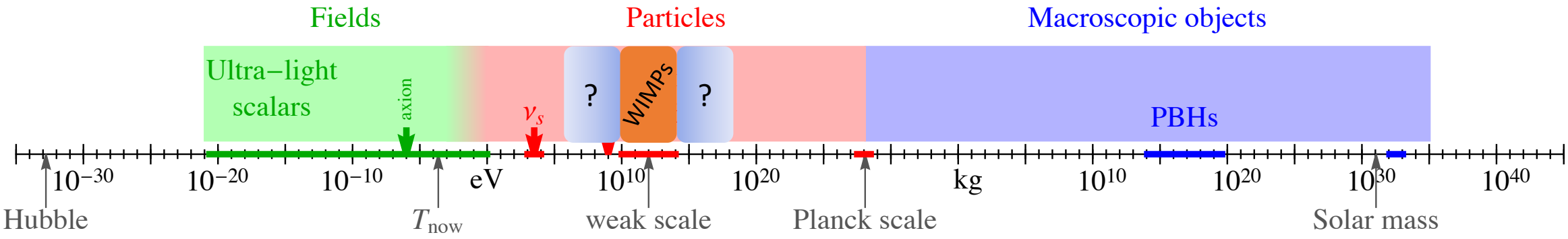

Introduction

- No WIMP signals observed in collider searches, direct and indirect detection…

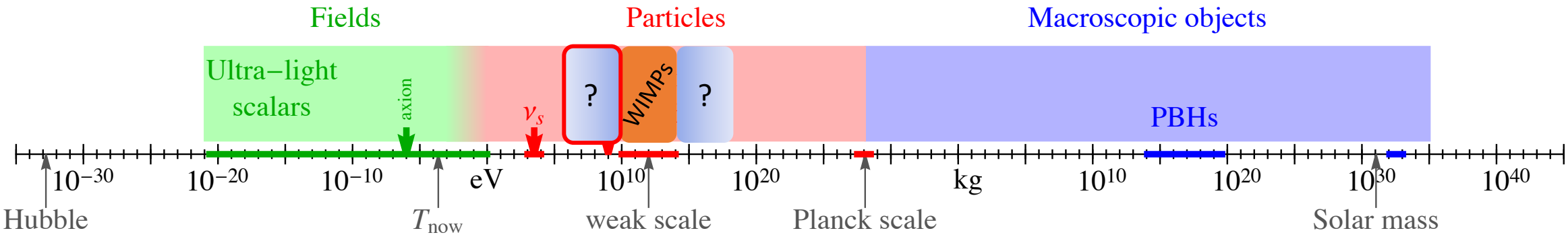

Introduction

- A lot of ‘light’ DM models are well-motivated:

Introduction

- A lot of ‘light’ DM models are well-motivated:
  - Hidden sector/secluded DM
  - SIMP DM
  - Asymmetric DM
  - …

Introduction

- A lot of ‘light’ DM models are well-motivated:
  - Hidden sector/secluded DM
  - SIMP DM
  - Asymmetric DM
  - …
- Detection of light DM is however tricky…

Introduction

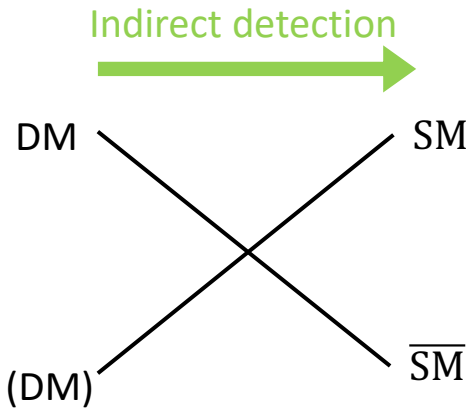

Issue in Indirect Detection:

Solar winds are a barrier to low-energy charged particles

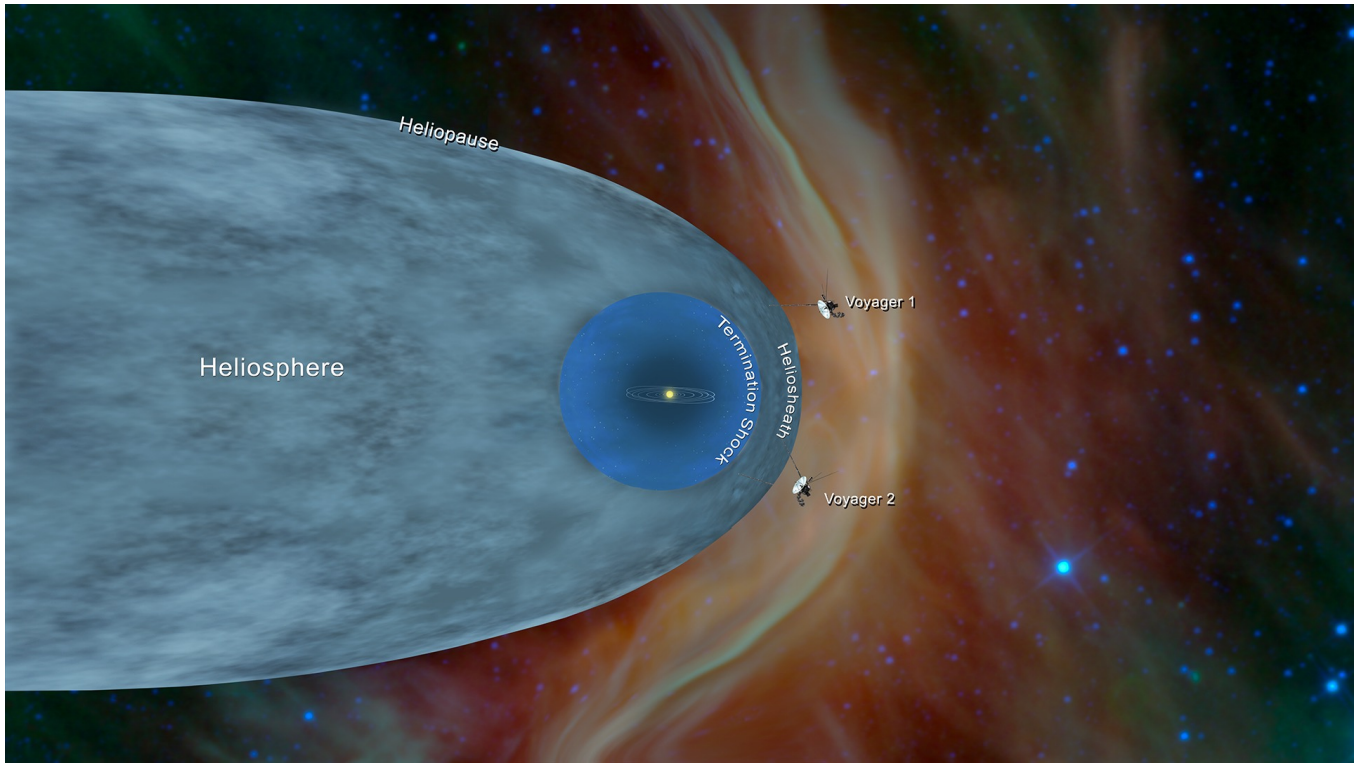

Introduction

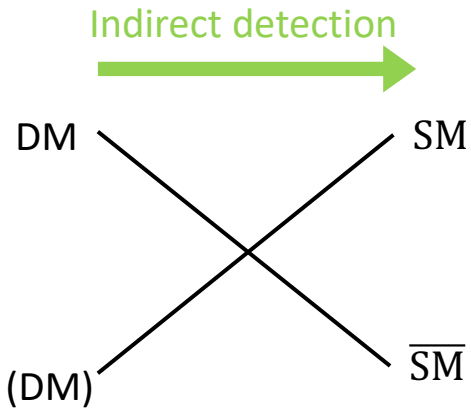

Issue in Indirect Detection:

Solar winds are a barrier to low-energy charged particles

Solutions:

- Look at Voyager1 & 2 data!
- What about photons?

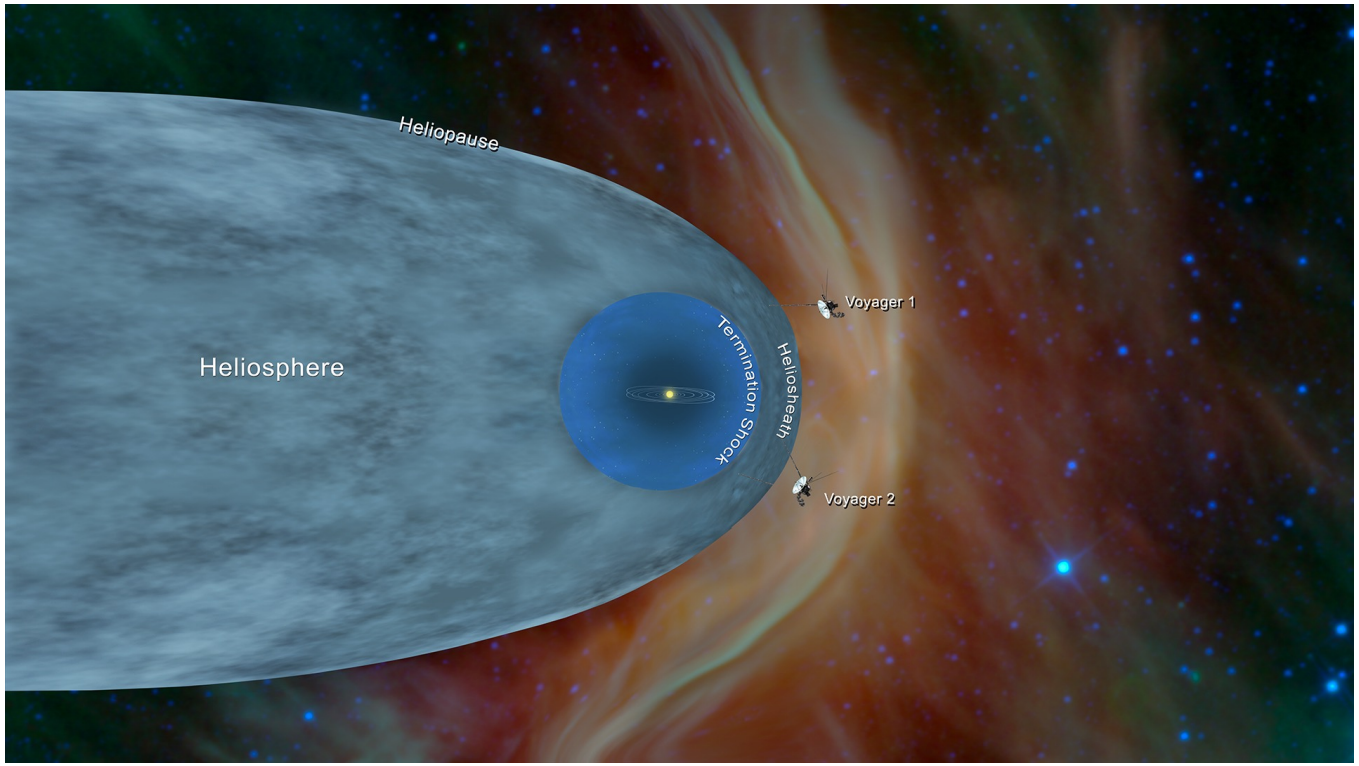

Introduction

- No data of quality for γ-rays between $\sim$ 100 keV – 100 MeV

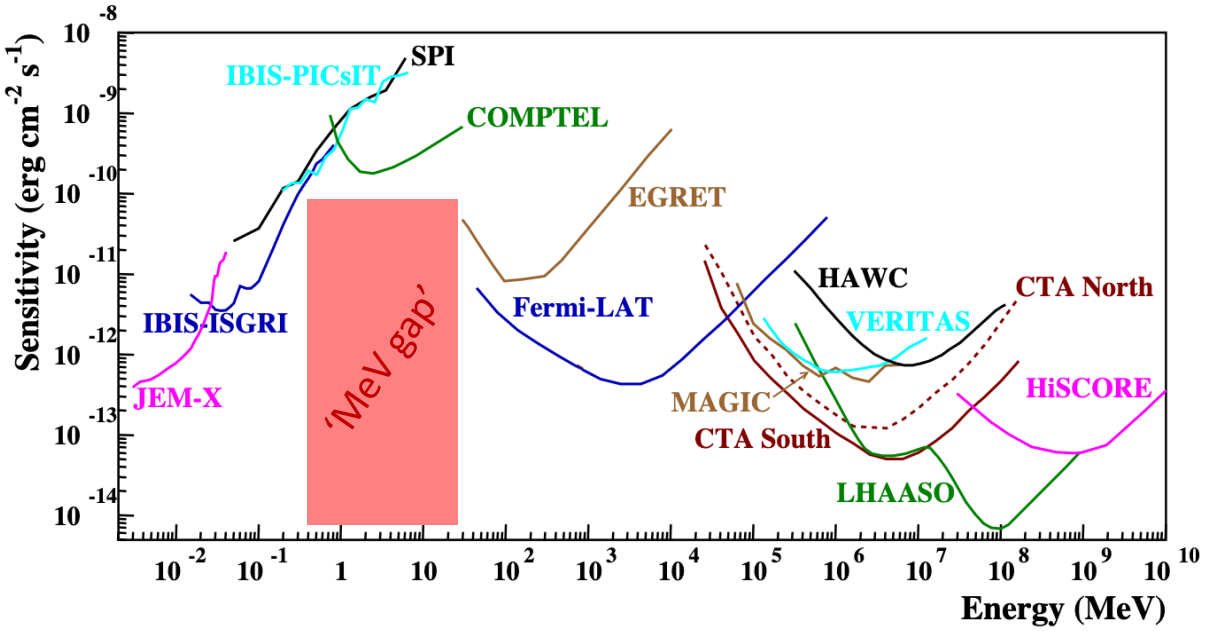

Adapted from De Angelis et al., AMEGO coll., 1611.02232

Introduction

- No data of quality for γ-rays between $\sim$ 100 keV – 100 MeV

- We focus on secondary emissions to circumvent this problem, and study light DM signals in the Milky Way using X-rays

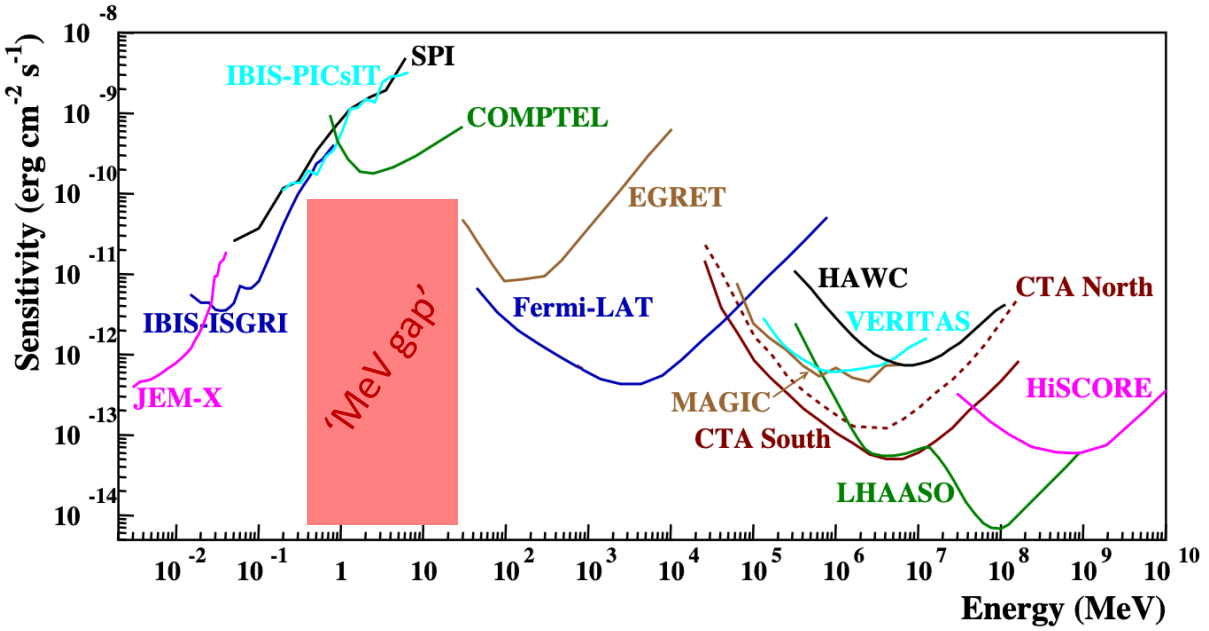

Adapted from De Angelis et al., AMEGO coll., 1611.02232

X-rays from DM destruction

(annihilation or decay)

X-rays from DM destruction

- There are a few ways to generate X-rays from DM destruction:

X-rays from DM destruction

- There are a few ways to generate X-rays from DM destruction:
  - Prompt emissions:
  - Secondary emissions (energy loss):

X-rays from DM destruction

- There are a few ways to generate X-rays from DM destruction:
  - Prompt emissions:
    - **Final state radiation** (FSR): DM (DM) $\rightarrow \mu^+\mu^-\gamma$
  - Secondary emissions (energy loss):

X-rays from DM destruction

- There are a few ways to generate X-rays from DM destruction:
  - Prompt emissions:
    - **Final state radiation** (FSR): DM (DM) $\rightarrow \mu^+\mu^-\gamma$
    - **Radiative decay** (Rad): DM (DM) $\rightarrow \mu^+\mu^- \rightarrow \mu^+ e^-\bar{\nu}_e\nu_\mu\gamma$
  - Secondary emissions (energy loss):

X-rays from DM destruction

- There are a few ways to generate X-rays from DM destruction:
  - Prompt emissions:
    - **Final state radiation** (FSR): DM (DM) $\rightarrow \mu^+\mu^-\gamma$
    - **Radiative decay** (Rad): DM (DM) $\rightarrow \mu^+\mu^- \rightarrow \mu^+ e^-\bar{\nu}_e\nu_\mu\gamma$
  - Secondary emissions (energy loss):
    - **Inverse-Compton scattering**: up-scattering of ambient photons thanks to $e^\pm$

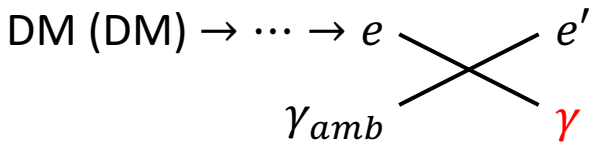

X-rays from DM destruction

- We consider the following mass range for DM:

$$1\ \mathrm{MeV} < m_{DM} < 5\ \mathrm{GeV}$$

X-rays from DM destruction

- We consider the following mass range for DM:

$$1\ \mathrm{MeV} < m_{DM} < 5\ \mathrm{GeV}$$

- Kinematically open primary channels that produce $e^{\pm}$ one way or another:

X-rays from DM destruction

- We consider the following mass range for DM:

$$1\ \mathrm{MeV} < m_{DM} < 5\ \mathrm{GeV}$$

- Kinematically open primary channels that produce $e^{\pm}$ one way or another:
  - DM (DM) $\rightarrow e^{+}e^{-}$

X-rays from DM destruction

- We consider the following mass range for DM:

$$1\ \mathrm{MeV} < m_{DM} < 5\ \mathrm{GeV}$$

- Kinematically open primary channels that produce $e^{\pm}$ one way or another:
  - DM (DM) $\rightarrow e^{+}e^{-}$
  - DM (DM) $\rightarrow \mu^{+}\mu^{-}$ $\quad (\mu^{\pm} \rightarrow e^{\pm}\nu_e\nu_\mu\ @ \sim 100\%)$

X-rays from DM destruction

- We consider the following mass range for DM:

$$1\ \mathrm{MeV} < m_{DM} < 5\ \mathrm{GeV}$$

- Kinematically open primary channels that produce $e^{\pm}$ one way or another:
  - DM (DM) $\rightarrow e^{+}e^{-}$
  - DM (DM) $\rightarrow \mu^{+}\mu^{-}$ $\quad (\mu^{\pm} \rightarrow e^{\pm}\nu_e\nu_\mu\ @ \sim 100\%)$
  - DM (DM) $\rightarrow \pi^{+}\pi^{-}$ $\quad (\pi^{\pm} \rightarrow \mu^{\pm}\nu_\mu \quad @ \sim 100\%)$

X-rays from DM destruction

- Differential flux of photons from prompt emissions:

X-rays from DM destruction

- Differential flux of photons from prompt emissions:

$$f = \text{FSR, Rad} \qquad \frac{d\Phi_{f,\gamma}}{dE_\gamma d\Omega} = \frac{1}{4\pi}\frac{dN_\gamma^f}{dE_\gamma} \times \begin{cases} \frac{1}{2}\frac{\langle\sigma v\rangle}{m_{DM}^2}\int_{l.o.s.}\rho_{DM}^2 ds & \text{(annihilation)} \\ \frac{\Gamma}{m_{DM}}\int_{l.o.s.}\rho_{DM} ds & \text{(decay)} \end{cases}$$

X-rays from DM destruction

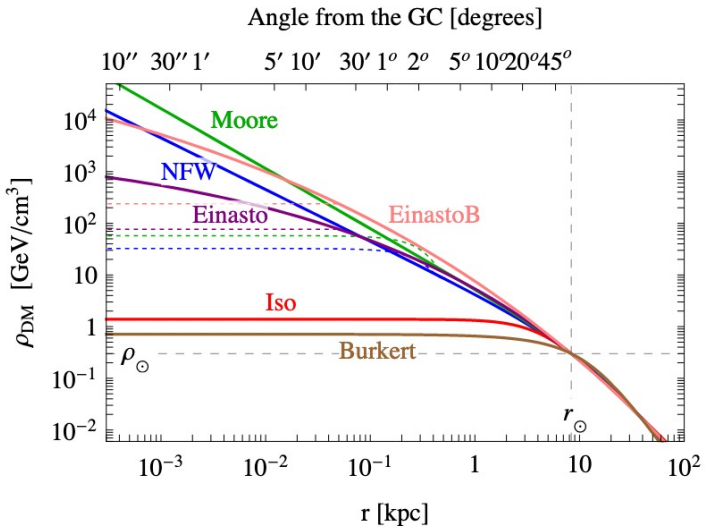

Cirelli et al., 1012.4515

- Differential flux of photons from prompt emissions:

$f = \text{FSR, Rad}$

$$\frac{d\Phi_{f,\gamma}}{dE_\gamma d\Omega} = \frac{1}{4\pi}\frac{dN_\gamma^f}{dE_\gamma} \times \begin{cases} \frac{1}{2}\frac{\langle\sigma v\rangle}{m_{DM}^2}\int_{l.o.s.}\rho_{DM}^2 ds & \text{(annihilation)} \\ \frac{\Gamma}{m_{DM}}\int_{l.o.s.}\rho_{DM} ds & \text{(decay)} \end{cases}$$

X-rays from DM destruction

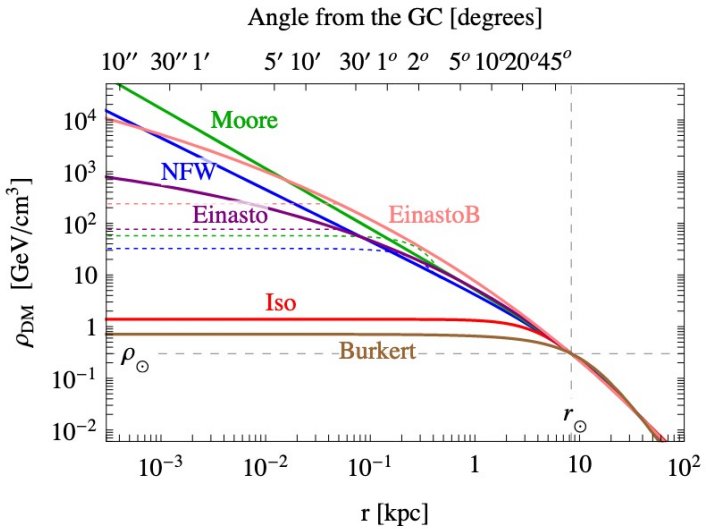

Cirelli et al., 1012.4515

- Differential flux of photons from prompt emissions:

$f = \text{FSR, Rad}$

$$\frac{d\Phi_{f,\gamma}}{dE_\gamma d\Omega} = \frac{1}{4\pi}\frac{dN_\gamma^f}{dE_\gamma} \times \begin{cases} \frac{1}{2}\frac{\langle\sigma v\rangle}{m_{DM}^2}\int_{l.o.s.}\rho_{DM}^2 ds & \text{(annihilation)} \\ \frac{\Gamma}{m_{DM}}\int_{l.o.s.}\rho_{DM} ds & \text{(decay)} \end{cases}$$

(Assuming DM is its own antiparticle)

X-rays from DM destruction

- DM-produced $e^{\pm}$ can up-scatter ambient photons up to X-ray energies

X-rays from DM destruction

- DM-produced $e^{\pm}$ can up-scatter ambient photons up to X-ray energies

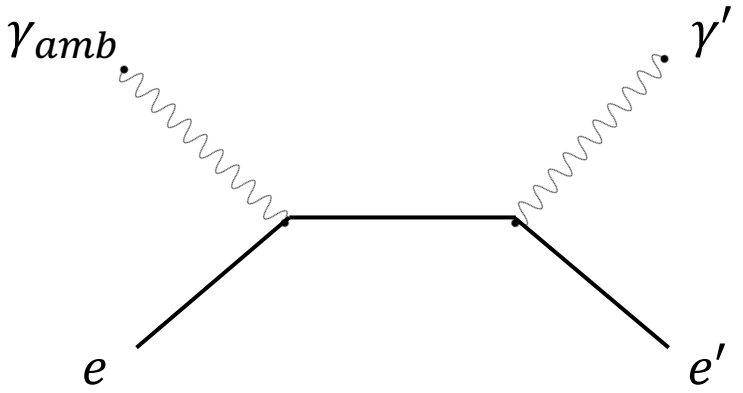

$$E_{\gamma'} \approx 4\gamma_e^2 E_{\gamma_{amb}} \qquad \gamma_e = \frac{E_e}{m_e}$$

X-rays from DM destruction

- DM-produced $e^{\pm}$ can up-scatter ambient photons up to X-ray energies

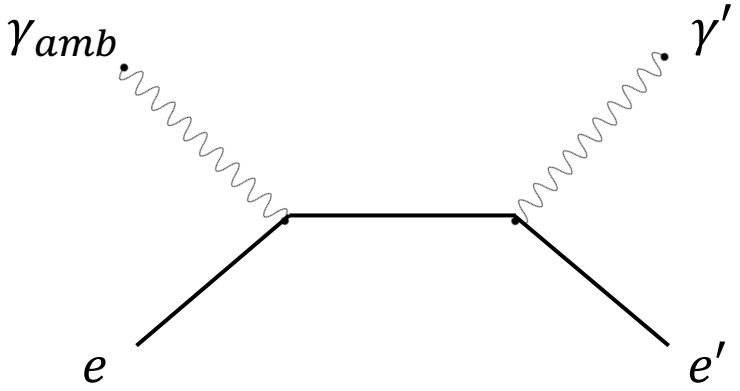

$$E_{\gamma'} \approx 4\gamma_e^2 E_{\gamma_{amb}} \qquad \gamma_e = \frac{E_e}{m_e}$$

- Ambient photons are: **CMB**, **dust-rescattered IR** and **optical starlight (SL)**
- Energy range $\sim$ 0.1 meV to 10 eV

X-rays from DM destruction

- DM-produced $e^{\pm}$ can up-scatter ambient photons up to X-ray energies

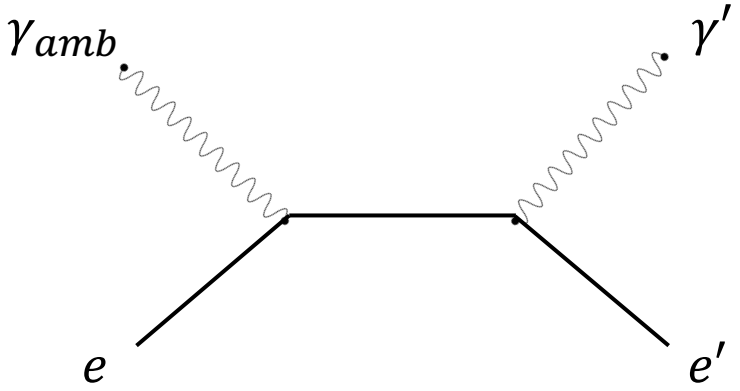

$$E_{\gamma'} \approx 4\gamma_e^2 E_{\gamma_{amb}} \qquad \gamma_e = \frac{E_e}{m_e}$$

For a CMB photon up-scattered by a 1 GeV $e^{\pm}$:

$$E_{\gamma_{amb}} \approx 0.2\ \mathrm{meV} \rightarrow E_{\gamma'} \approx 3\ \mathrm{keV}$$

- Ambient photons are: **CMB**, **dust-rescattered IR** and **optical starlight (SL)**
- Energy range $\sim$ 0.1 meV to 10 eV

X-rays from DM destruction

- To compute the IC-scattered photon flux, we need a few ingredients:

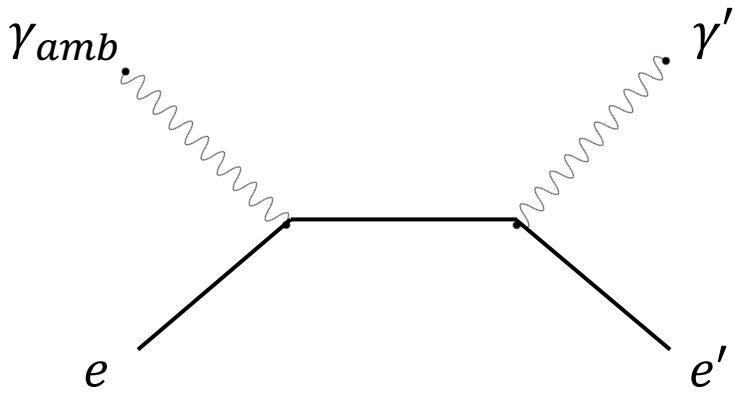

X-rays from DM destruction

- To compute the IC-scattered photon flux, we need a few ingredients:

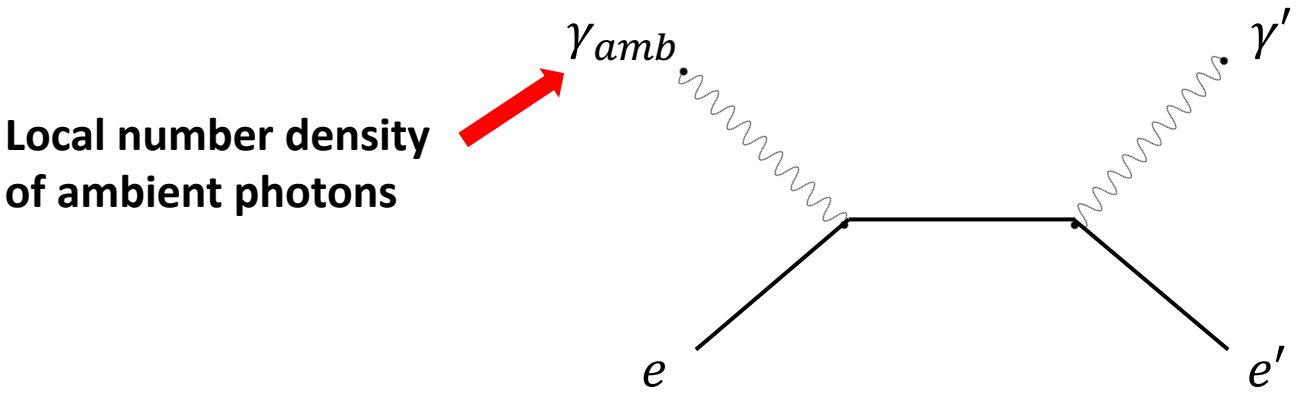

X-rays from DM destruction

- To compute the IC-scattered photon flux, we need a few ingredients:

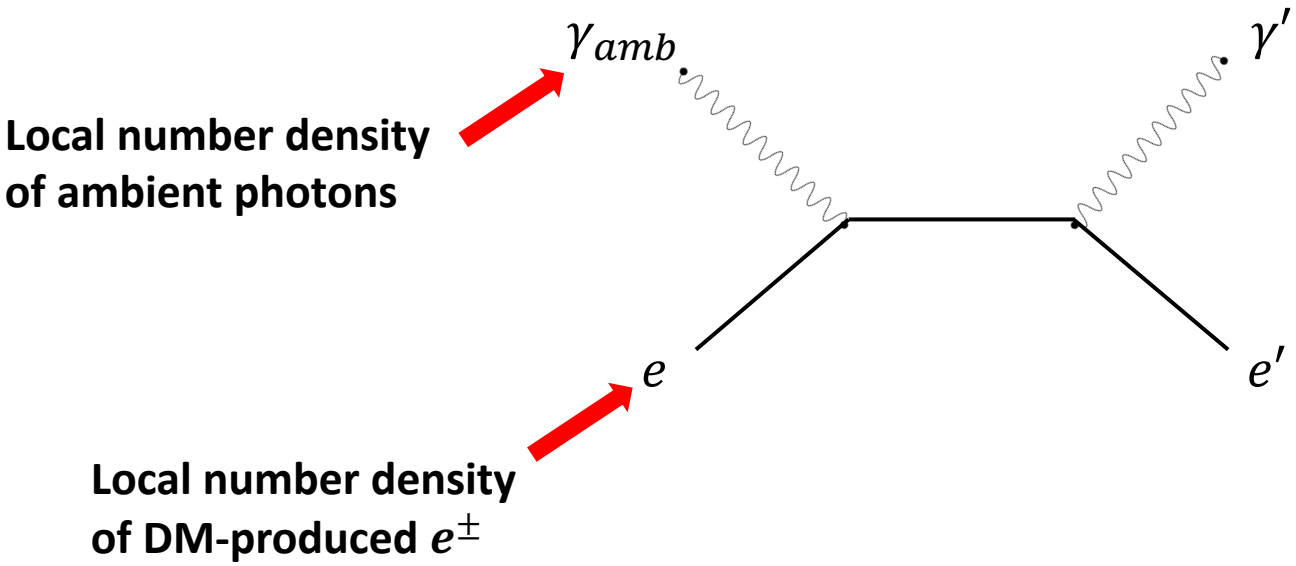

X-rays from DM destruction

- To compute the IC-scattered photon flux, we need a few ingredients:

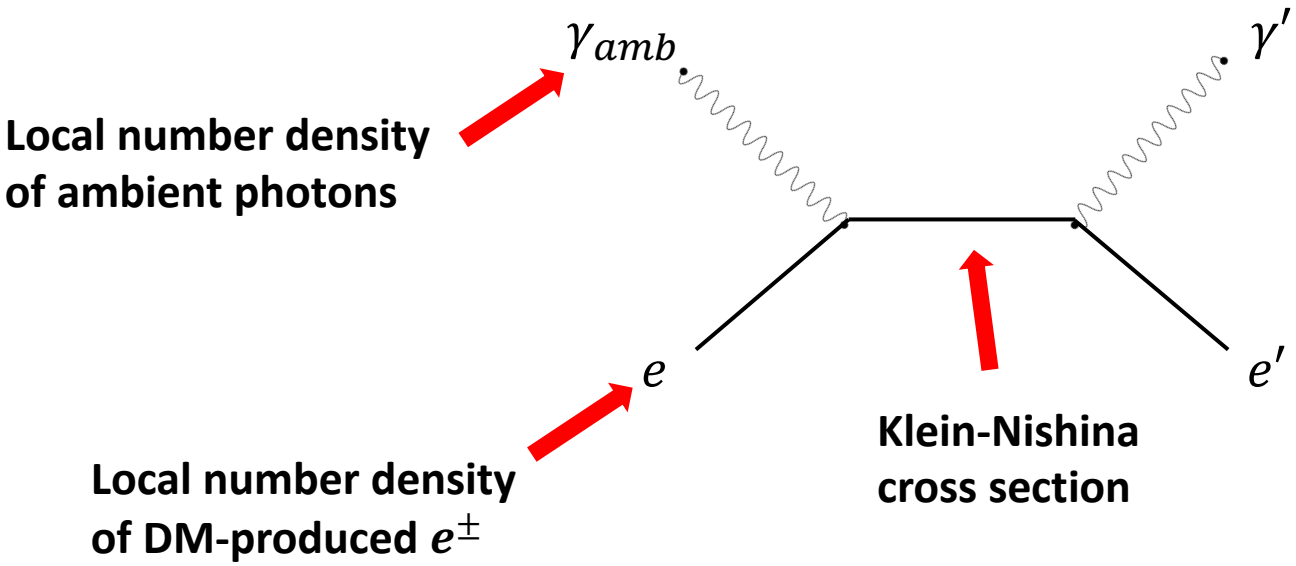

X-rays from DM destruction

- To compute the IC-scattered photon flux, we need a few ingredients:

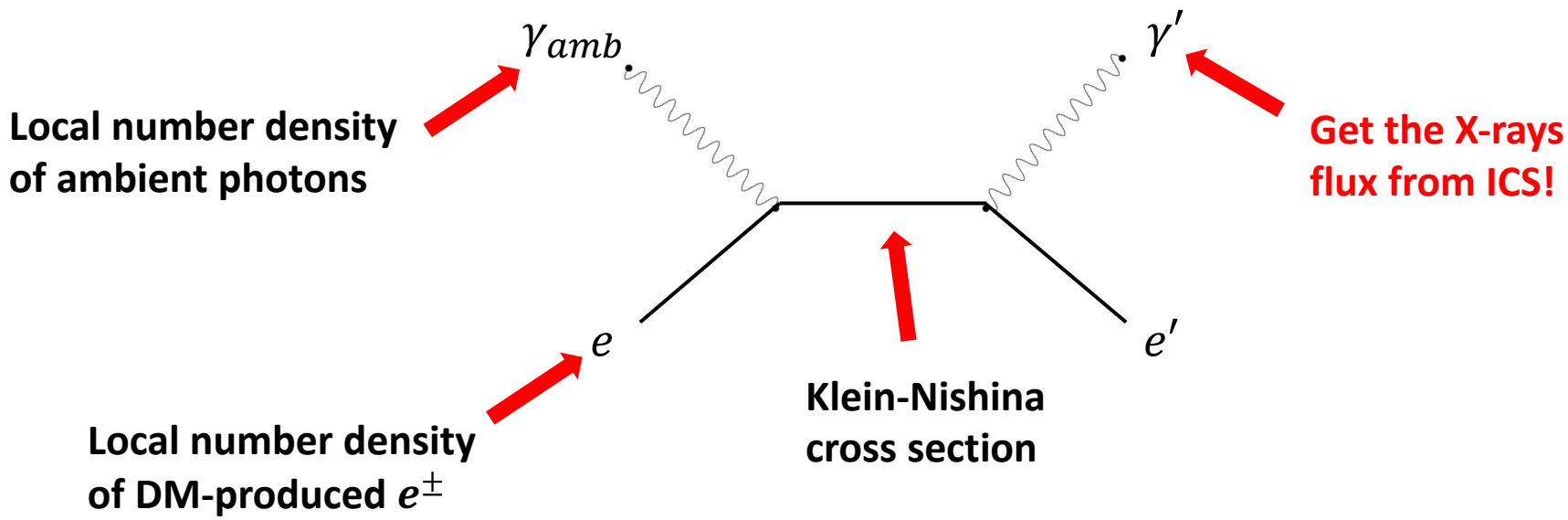

Analysis and results

Analysis and results

- In this study we keep a **conservative** approach:

Analysis and results

- In this study we keep a **conservative** approach:

$$\chi^2_{>}(p, m_{DM}) = \sum_{i \in \text{ bins}} \frac{\text{Max}\left(\Phi_{DM\gamma,i}(p, m_{DM}) - \Phi_i, 0\right)^2}{\sigma_i^2}$$

$$p = \langle \sigma v \rangle \, , \Gamma$$

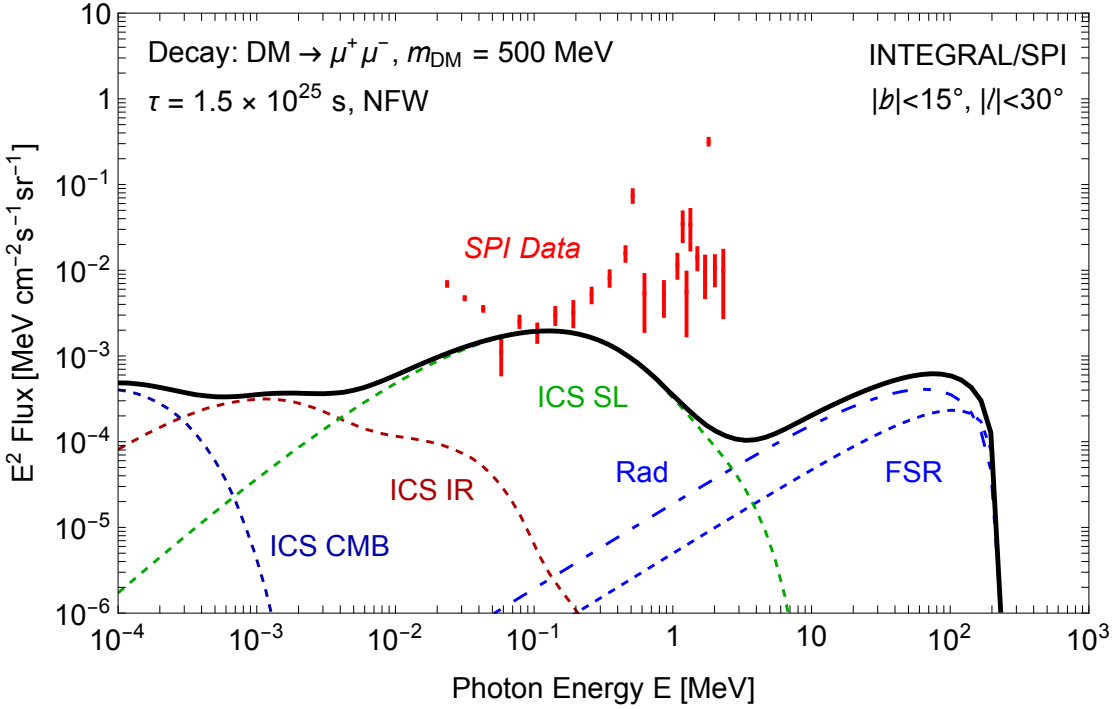

Analysis and results

- In this study we keep a **conservative** approach:

$$\chi^2_{>}(p, m_{DM}) = \sum_{i \in \text{ bins}} \frac{\text{Max}\left(\Phi_{DM\gamma,i}(p, m_{DM}) - \Phi_i, 0\right)^2}{\sigma_i^2}$$

$$p = \langle \sigma v \rangle \, , \Gamma$$

- Impose a bound when $\chi^2_{>}(p, m_{DM}) \geq 4$

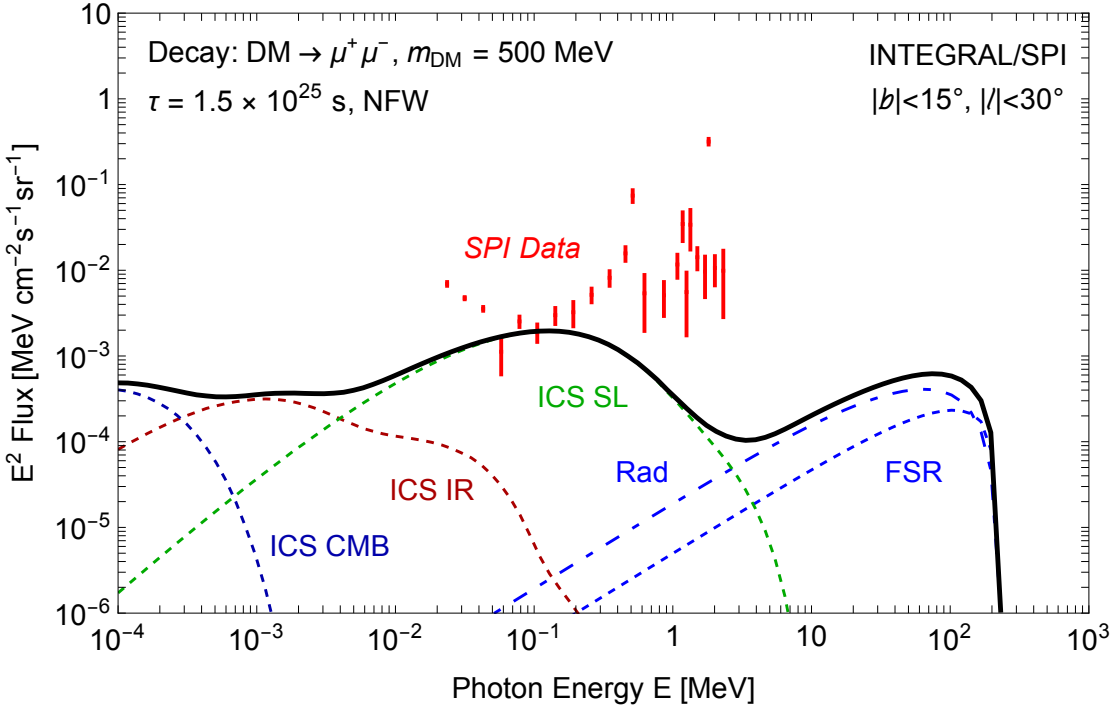

Analysis and results

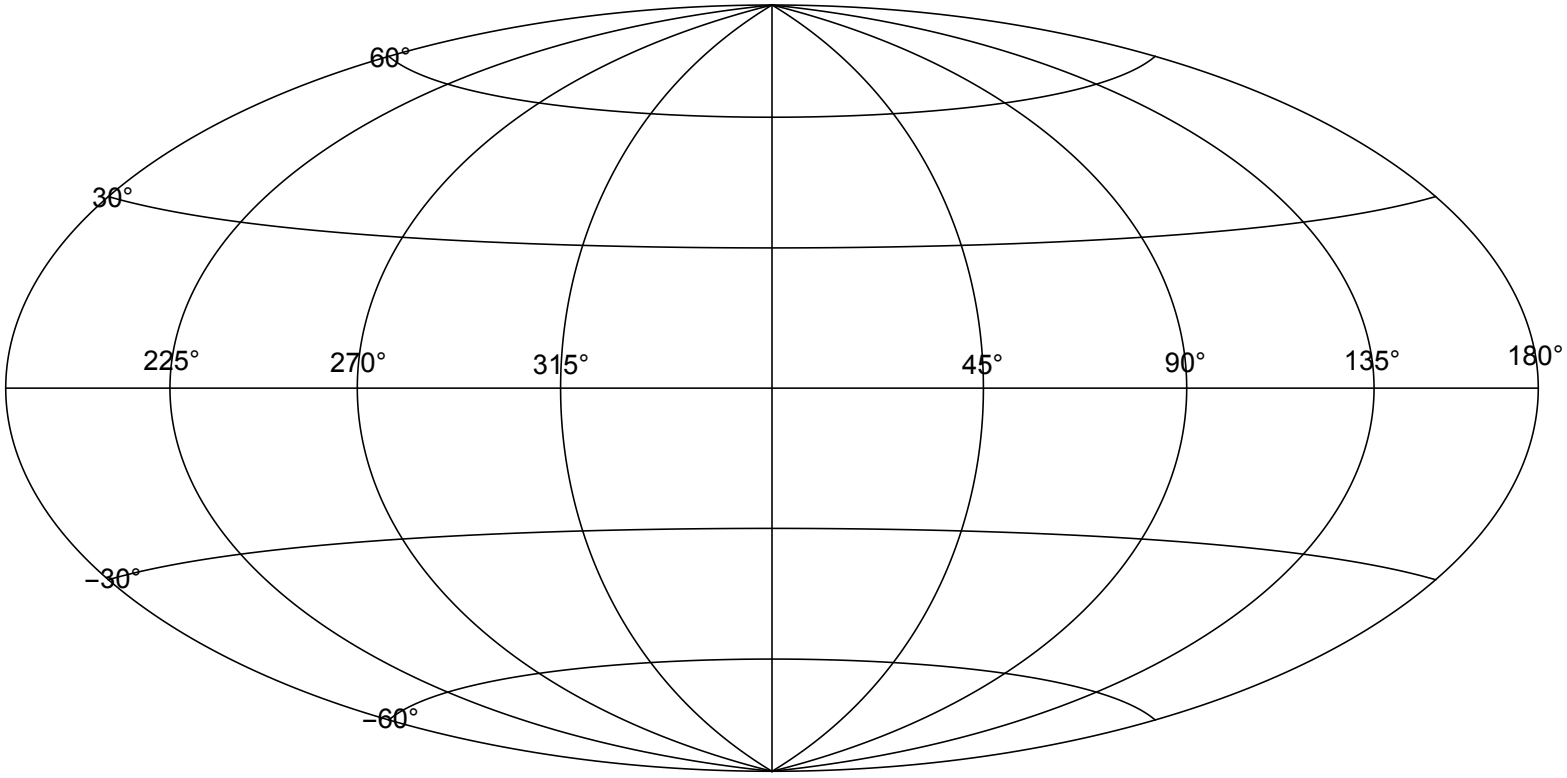

Analysis and results

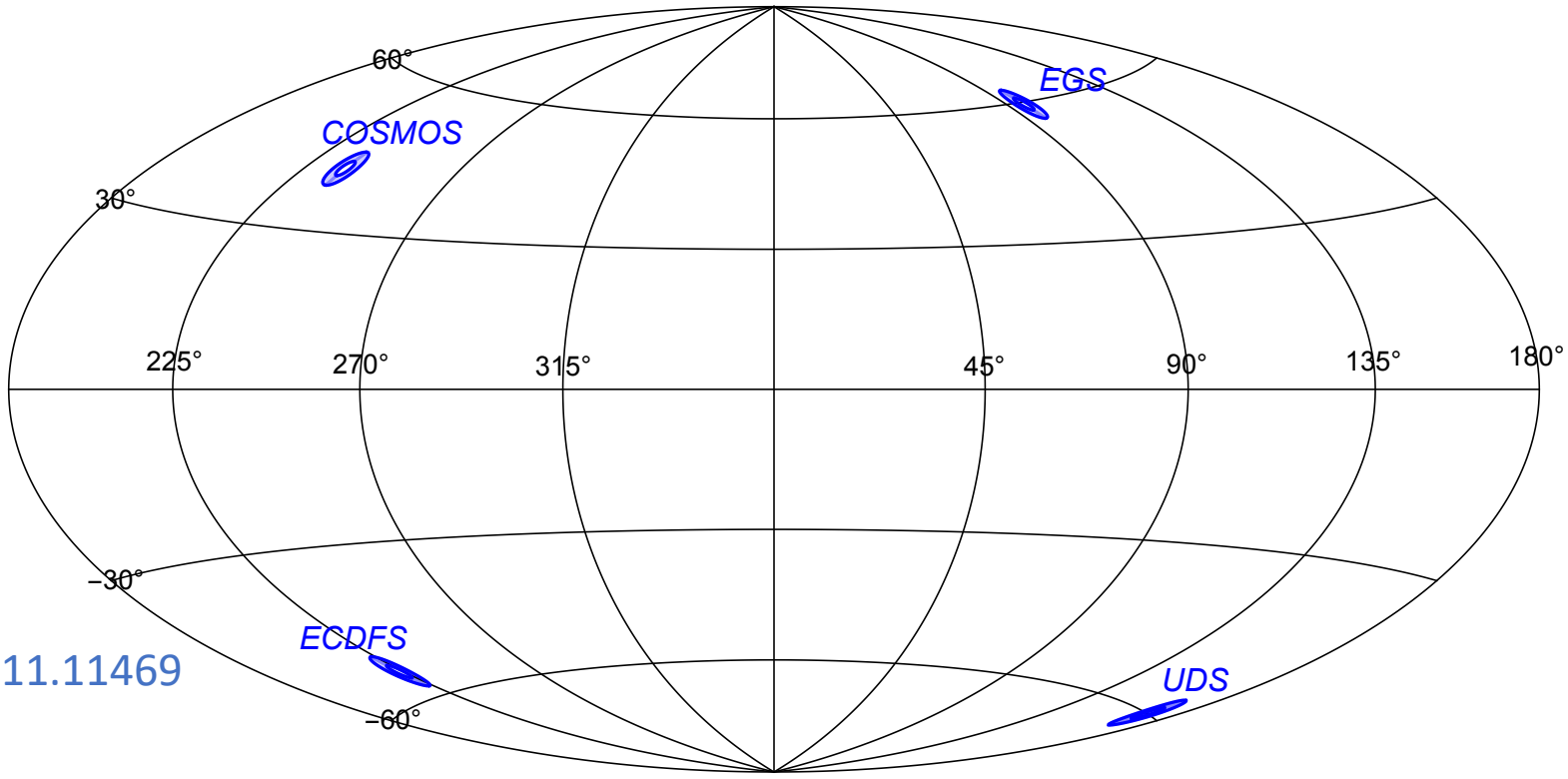

NuSTAR
2012-2018
Blank-sky fields
Krivonos et al., 2011.11469

Analysis and results

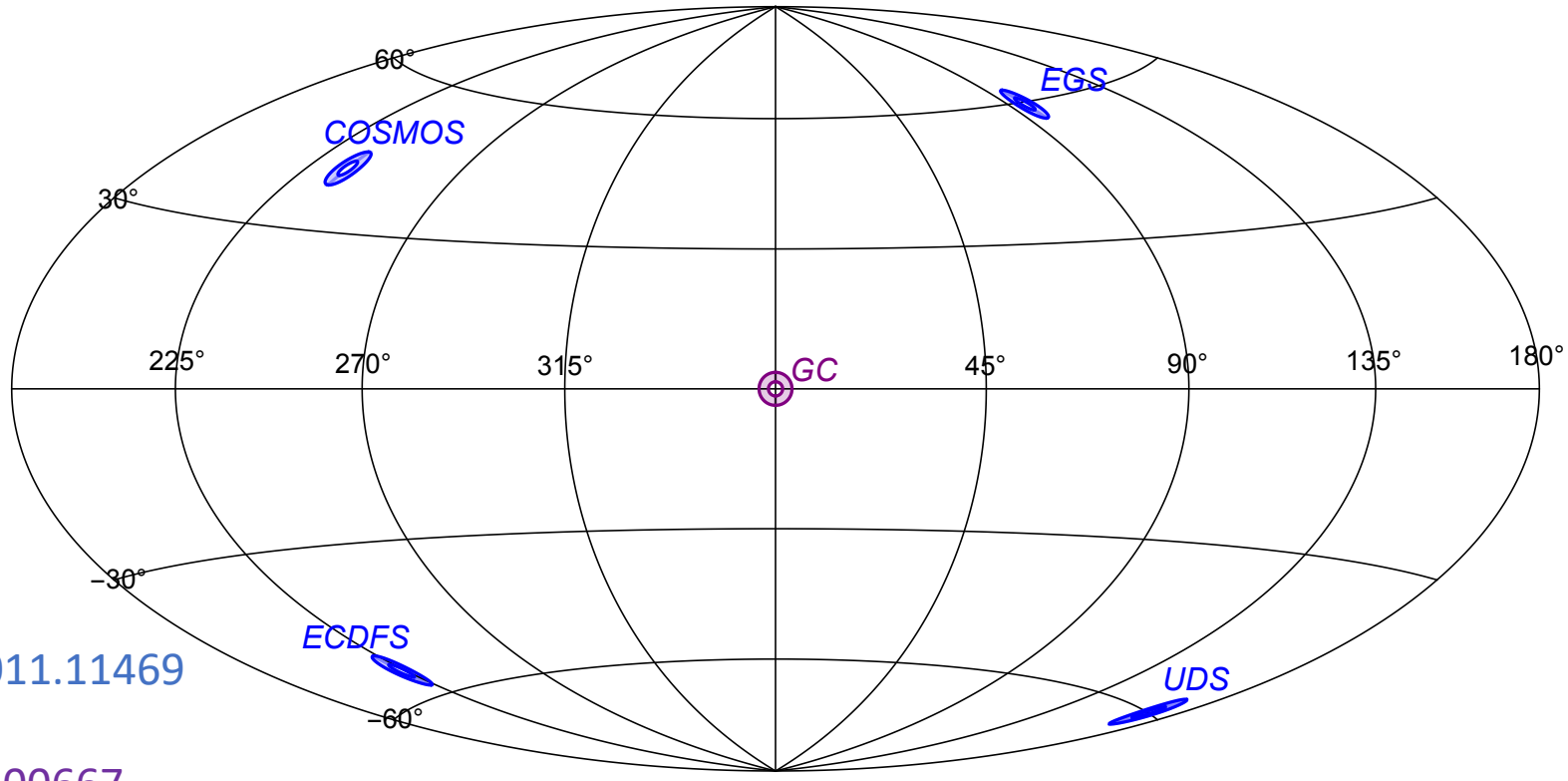

NuSTAR
2012-2018
Blank-sky fields
Krivonos et al., 2011.11469
GC observations
Perez et al., 1609.00667

Analysis and results

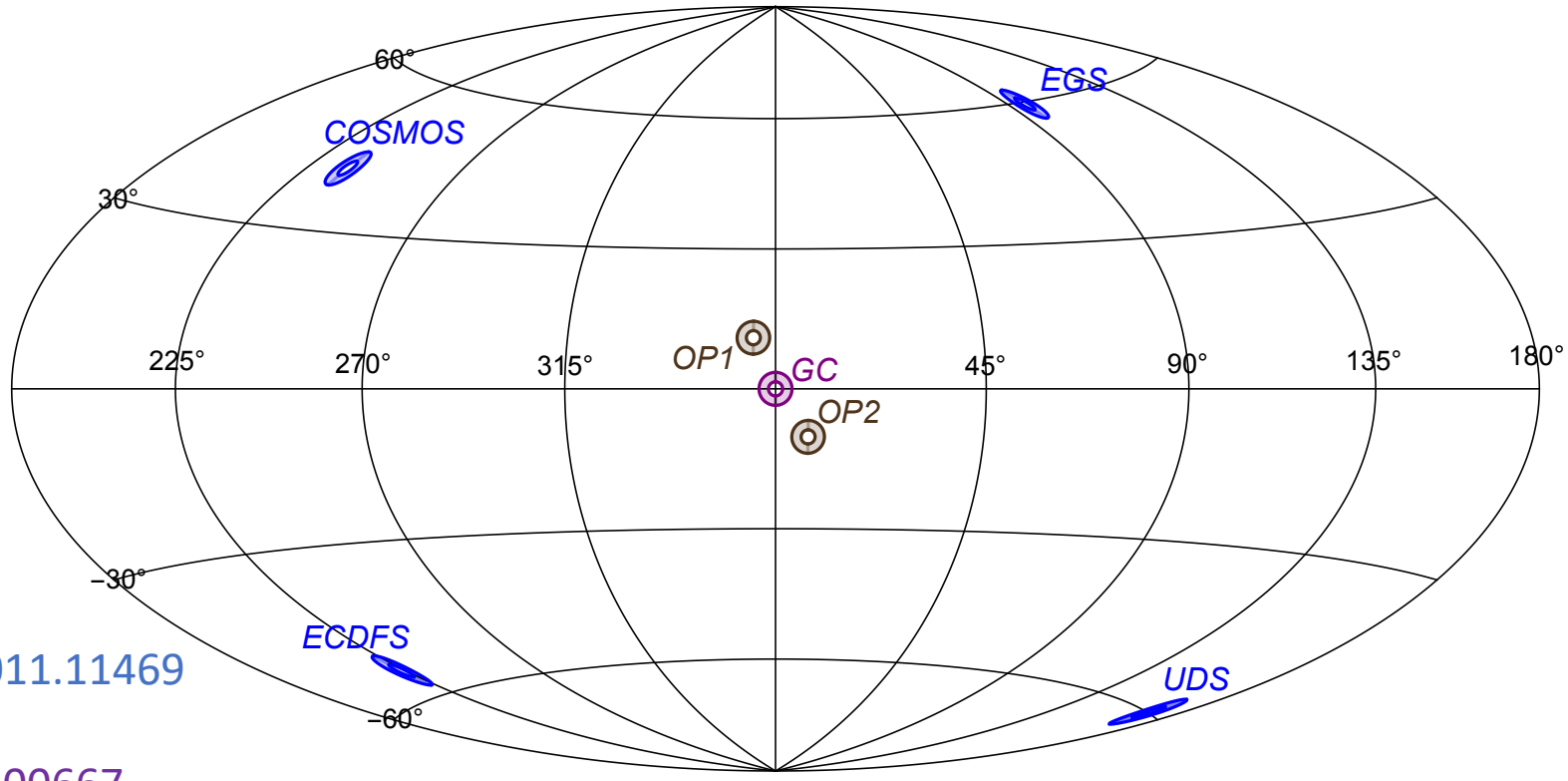

NuSTAR
2012-2018
Blank-sky fields
Krivonos et al., 2011.11469
GC observations
Perez et al., 1609.00667
Off-plane observations
Roach et al., 1908.09037

Analysis and results

INTEGRAL diffuse emission searches
2003-2009
Bouchet et al., INTEGRAL coll., 1107.0200

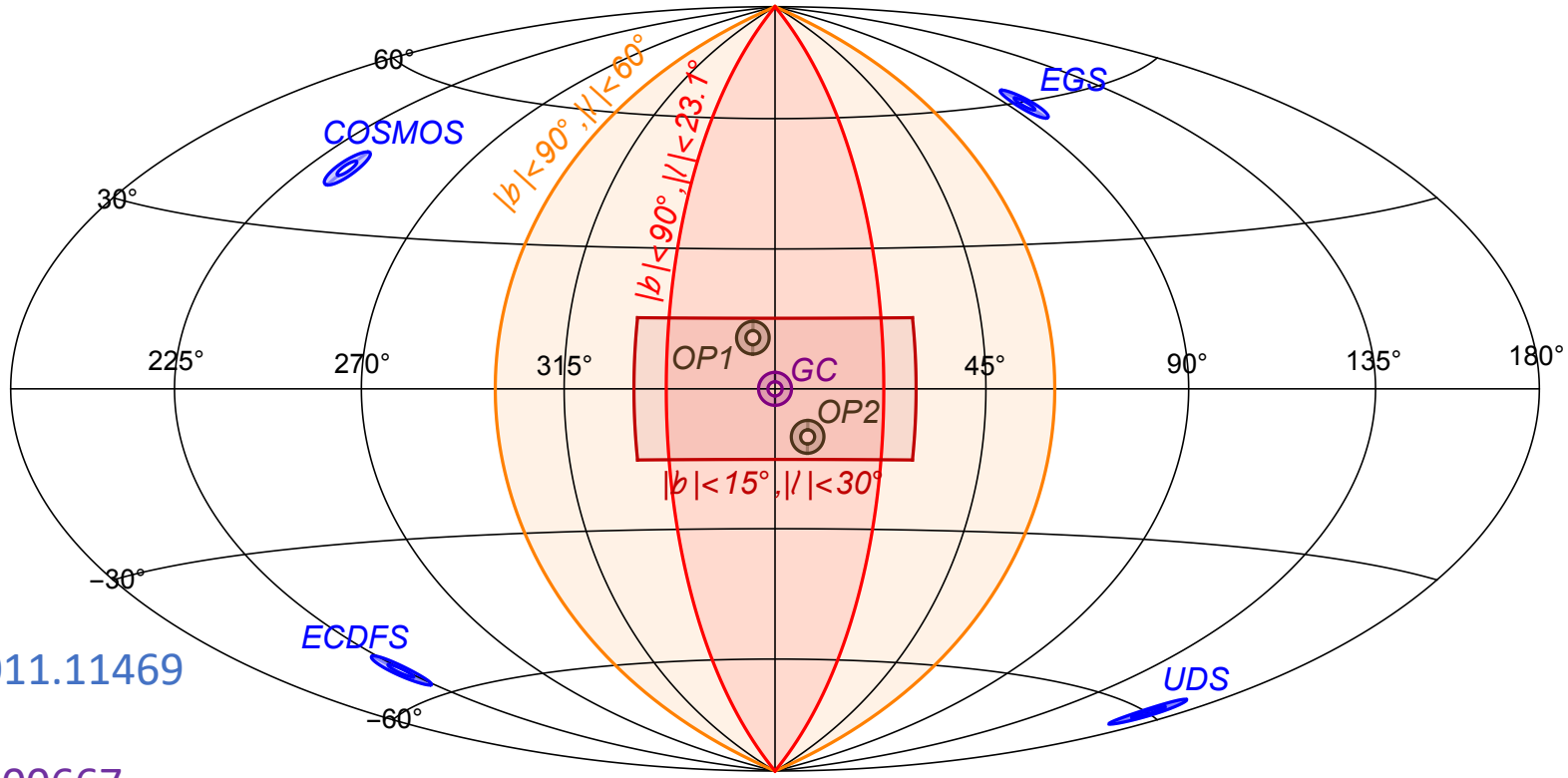

NuSTAR
2012-2018
Blank-sky fields
Krivonos et al., 2011.11469
GC observations
Perez et al., 1609.00667
Off-plane observations
Roach et al., 1908.09037

Analysis and results

INTEGRAL diffuse emission searches
2003-2009
Bouchet et al., INTEGRAL coll., 1107.0200

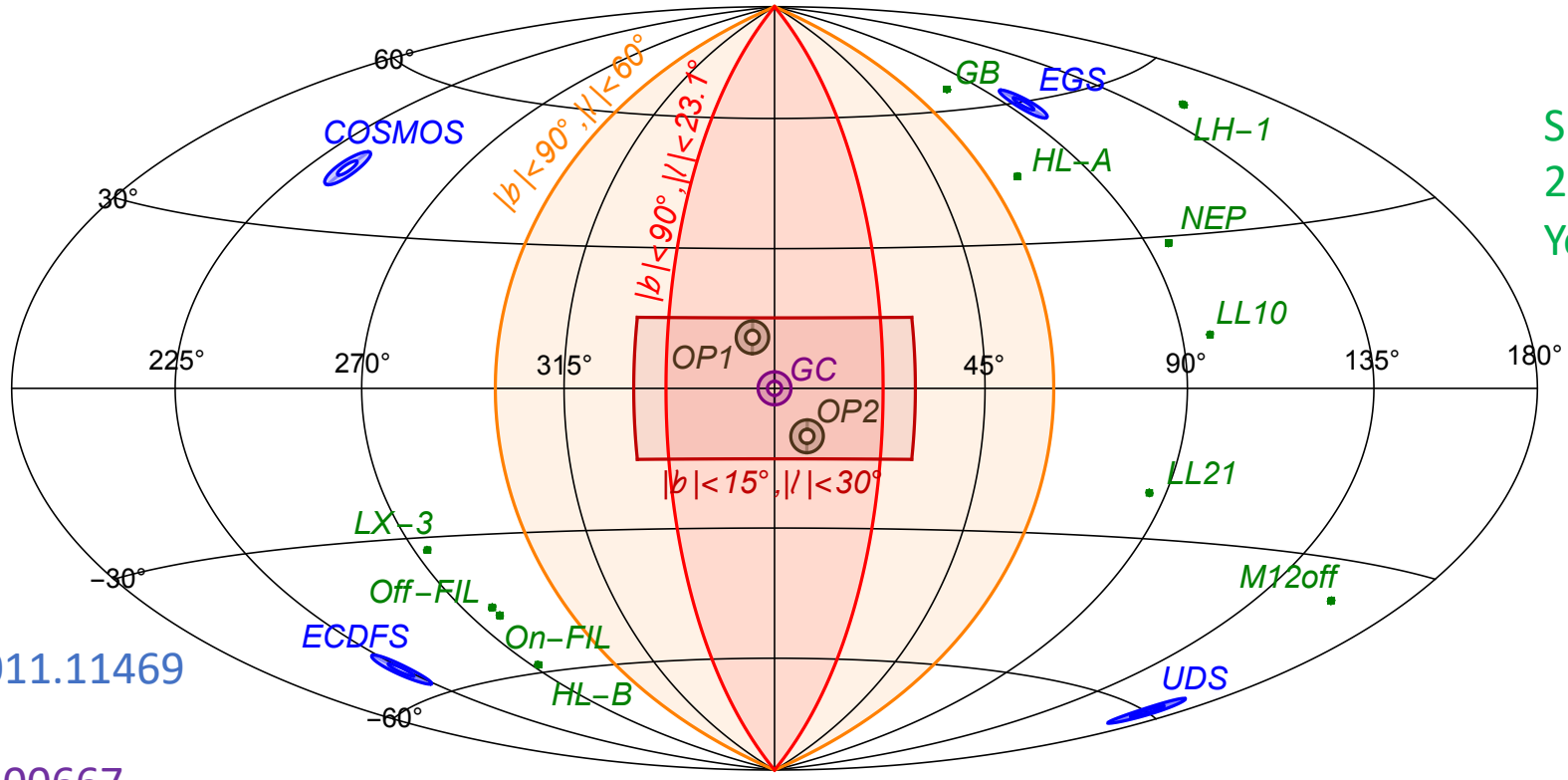

Suzaku high-latitude fields
2006-2008
Yoshino et al., 0903.2981

NuSTAR
2012-2018
Blank-sky fields
Krivonos et al., 2011.11469
GC observations
Perez et al., 1609.00667
Off-plane observations
Roach et al., 1908.09037

Analysis and results

INTEGRAL diffuse emission searches
2003-2009
Bouchet et al., INTEGRAL coll., 1107.0200

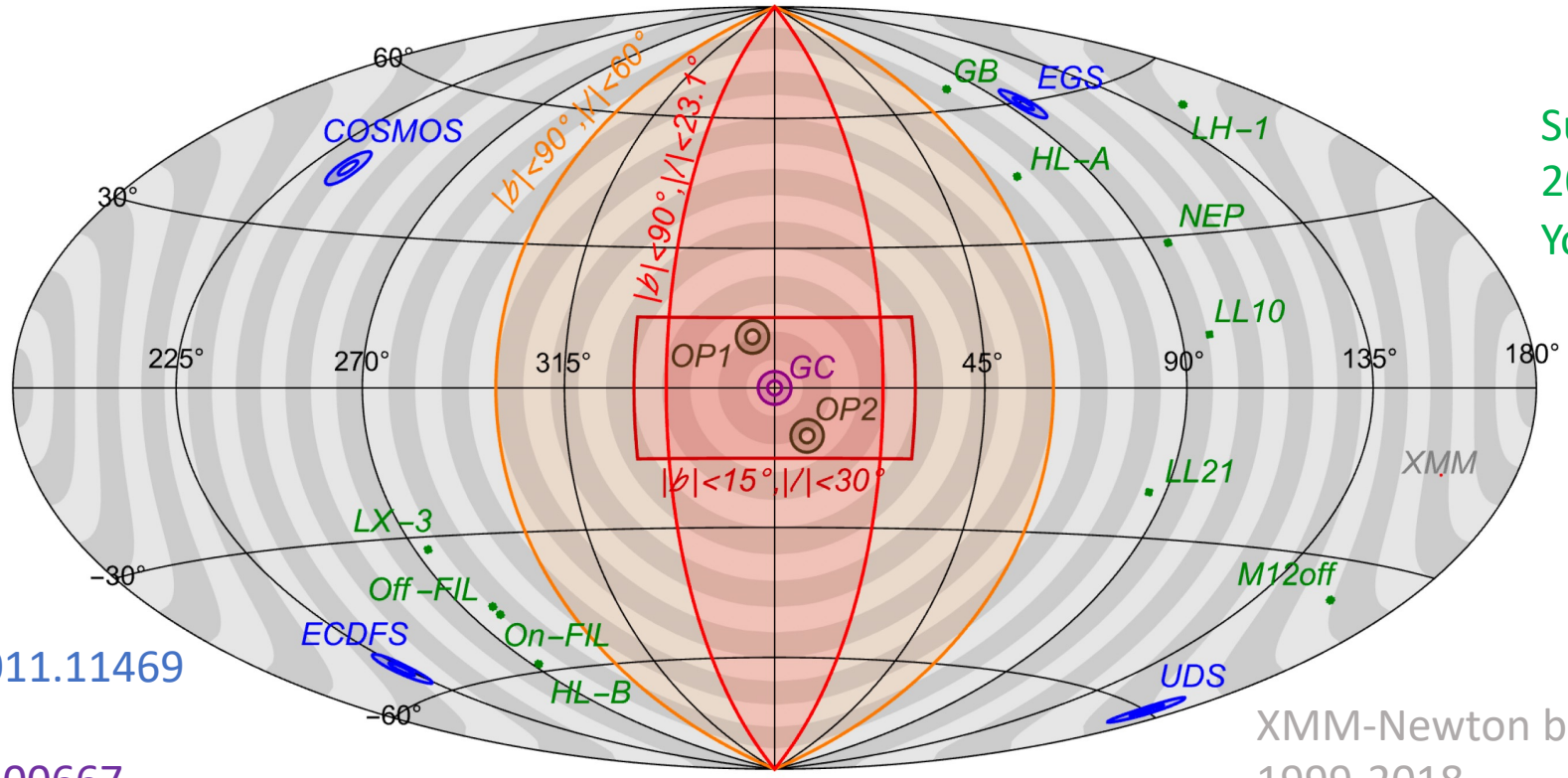

Suzaku high-latitude fields
2006-2008
Yoshino et al., 0903.2981

NuSTAR
2012-2018
Blank-sky fields
Krivonos et al., 2011.11469
GC observations
Perez et al., 1609.00667
Off-plane observations
Roach et al., 1908.09037

XMM-Newton blank-sky data
1999-2018
Foster et al., 2102.02207
https://github.com/bsafdi/XMM_BSO_DATA

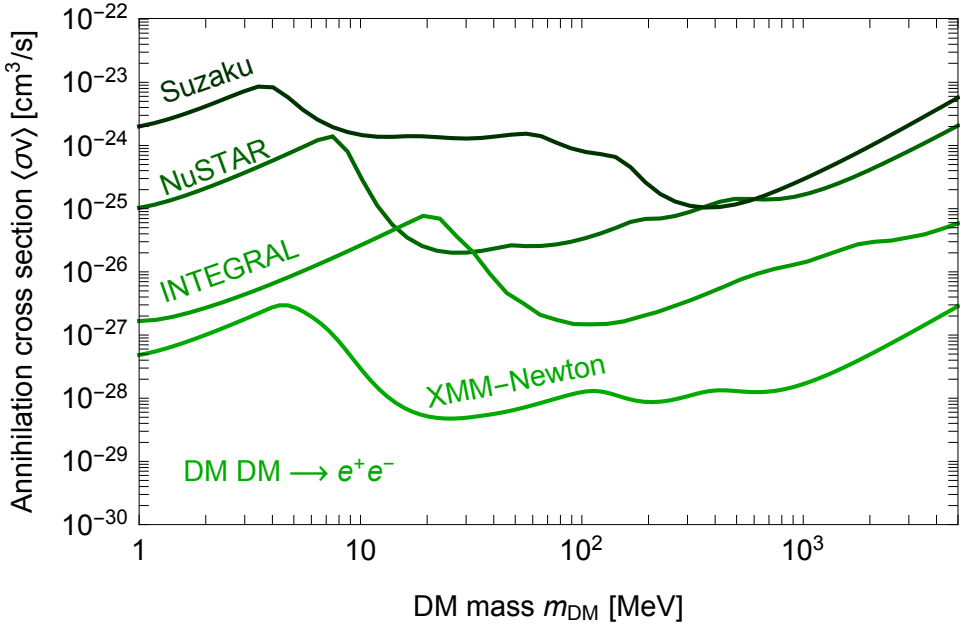
Annihilation cross section ⟨σv⟩ [cm³/s]
10⁻²²
10⁻²³
10⁻²⁴
10⁻²⁵
10⁻²⁶
10⁻²⁷
10⁻²⁸
10⁻²⁹
10⁻³⁰
Suzaku
NuSTAR
INTEGRAL
XMM–Newton
DM DM ⟶ e⁺e⁻
1
10
10²
10³
DM mass m_DM [MeV]

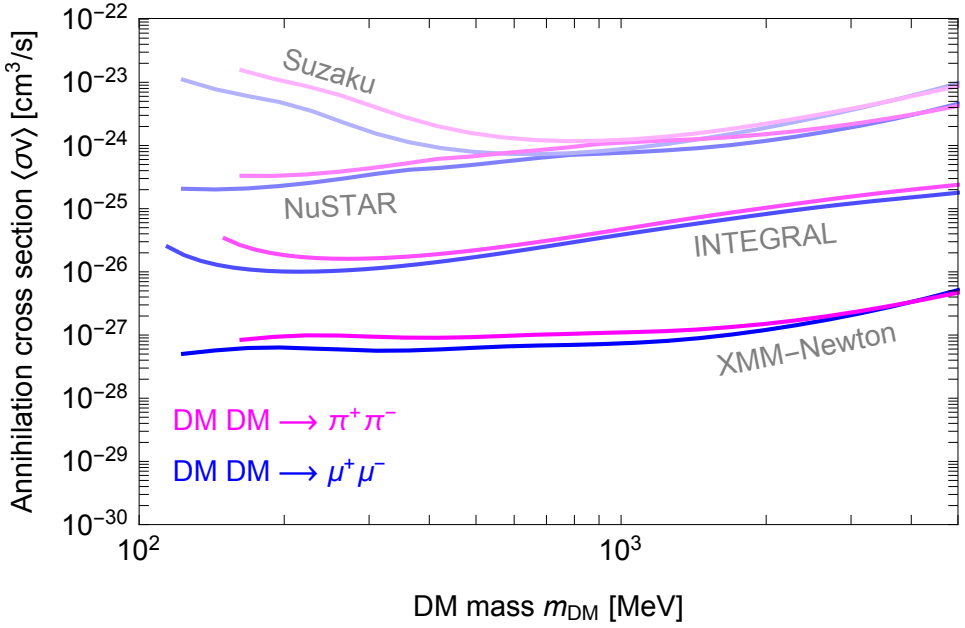
Annihilation cross section ⟨σv⟩ [cm³/s]
10⁻²²
10⁻²³
10⁻²⁴
10⁻²⁵
10⁻²⁶
10⁻²⁷
10⁻²⁸
10⁻²⁹
10⁻³⁰
Suzaku
NuSTAR
INTEGRAL
XMM–Newton
DM DM ⟶ π⁺π⁻
DM DM ⟶ μ⁺μ⁻
10²
10³
DM mass m_DM [MeV]

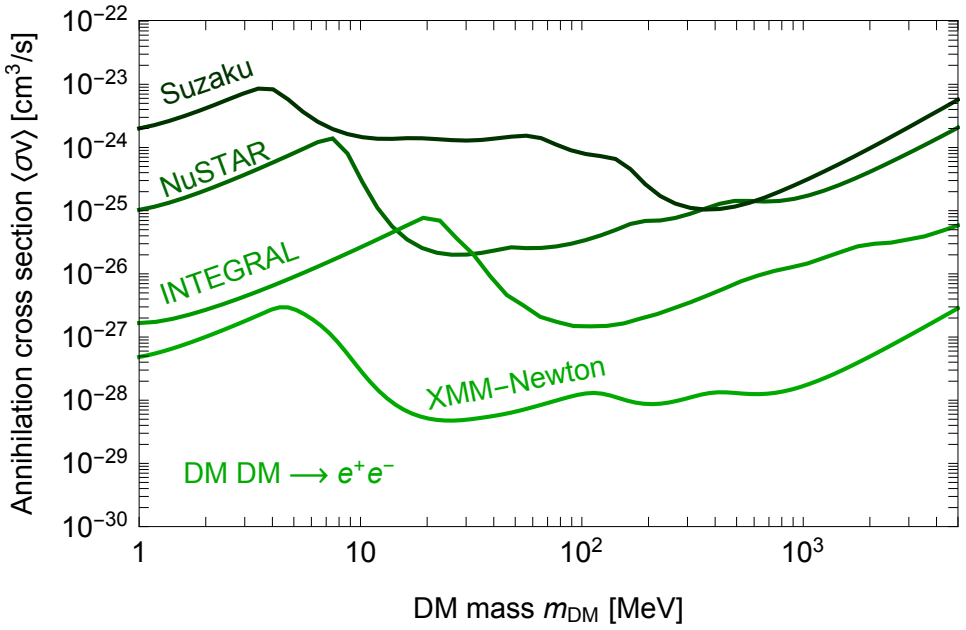
Annihilation cross section ⟨σv⟩ [cm³/s]
Suzaku
NuSTAR
INTEGRAL
XMM–Newton
DM DM ⟶ e⁺e⁻
DM mass m_DM [MeV]

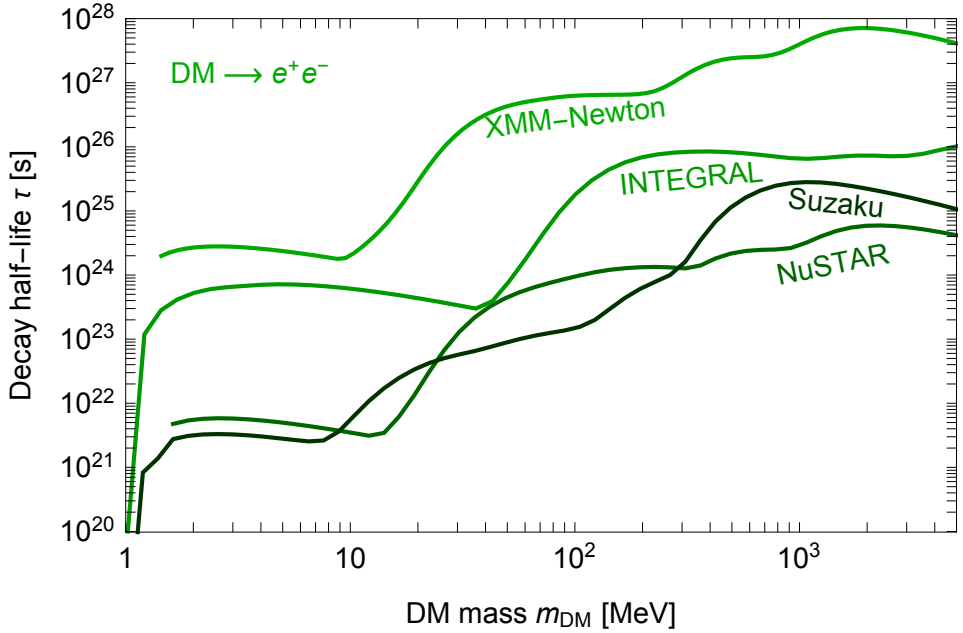
Decay half–life τ [s]
DM ⟶ e⁺e⁻
XMM–Newton
INTEGRAL
Suzaku
NuSTAR
DM mass m_DM [MeV]

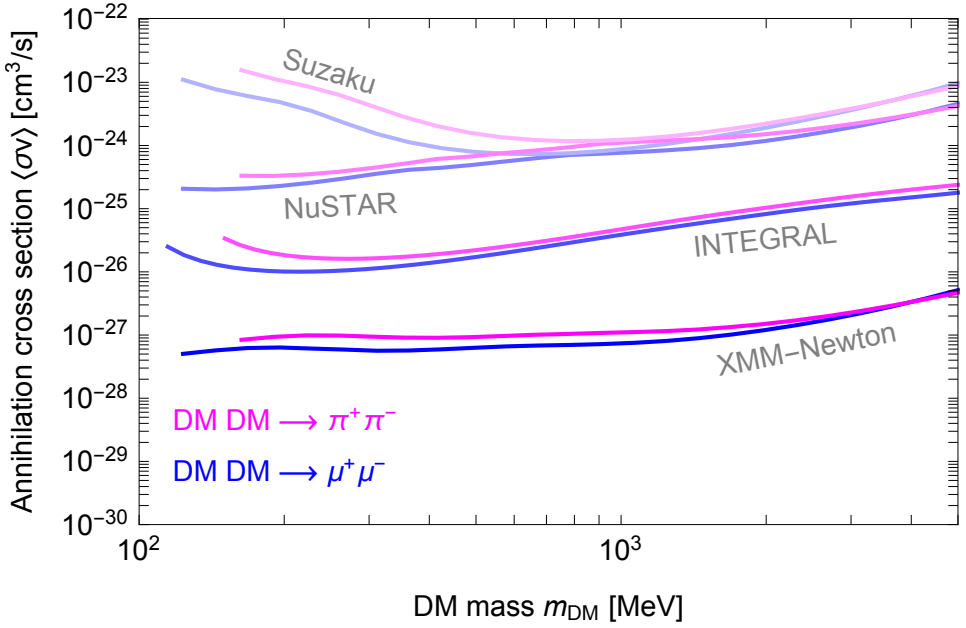
Annihilation cross section ⟨σv⟩ [cm³/s]
Suzaku
NuSTAR
INTEGRAL
XMM–Newton
DM DM ⟶ π⁺π⁻
DM DM ⟶ μ⁺μ⁻
DM mass m_DM [MeV]

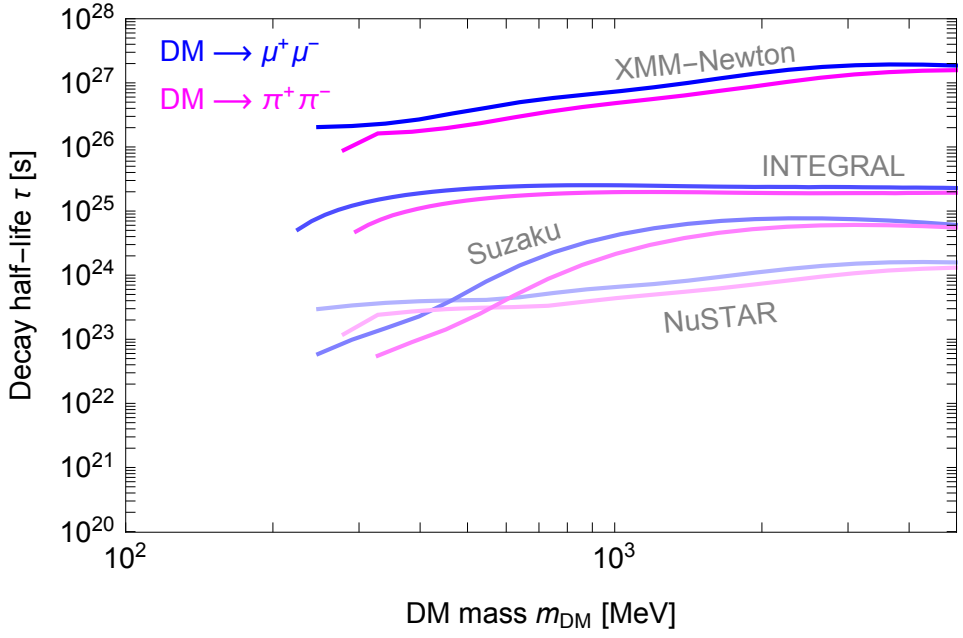
Decay half–life τ [s]
DM ⟶ μ⁺μ⁻
DM ⟶ π⁺π⁻
XMM–Newton
INTEGRAL
Suzaku
NuSTAR
DM mass m_DM [MeV]

Analysis and results

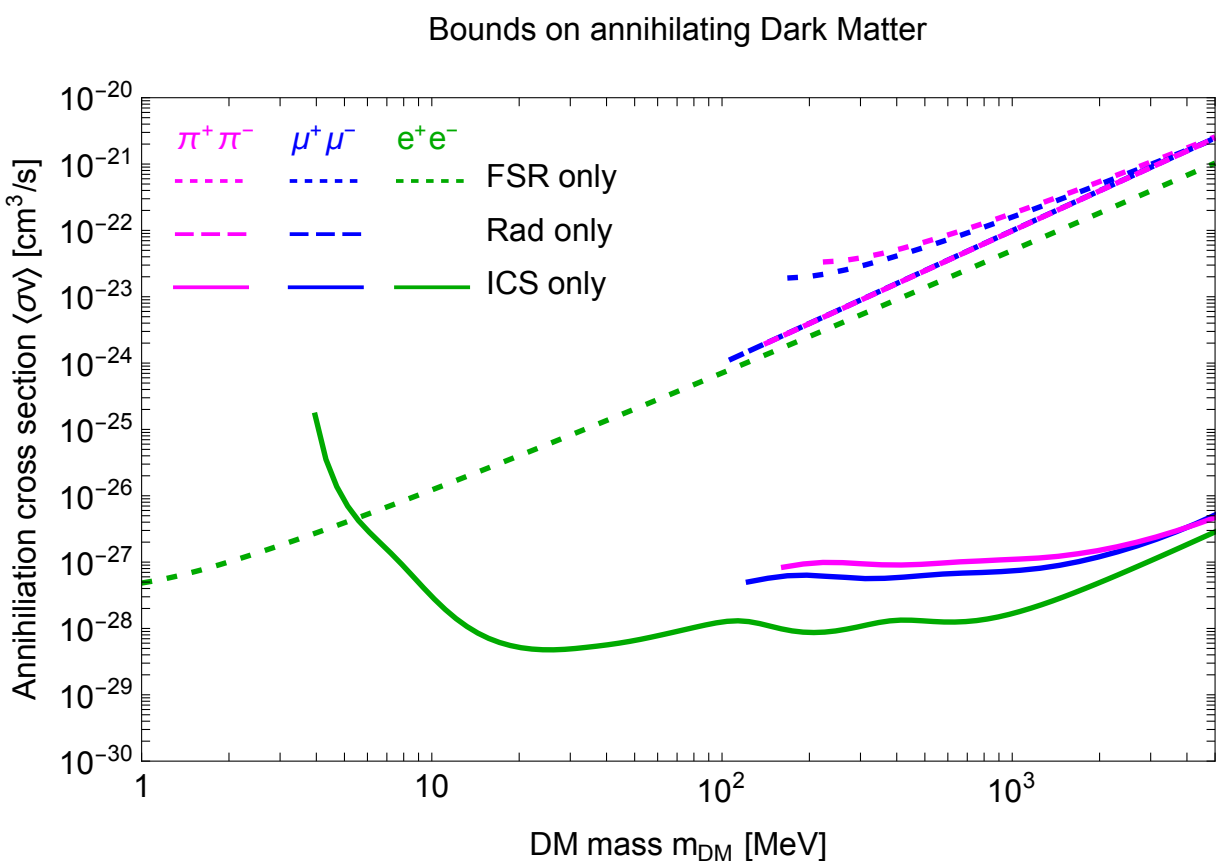

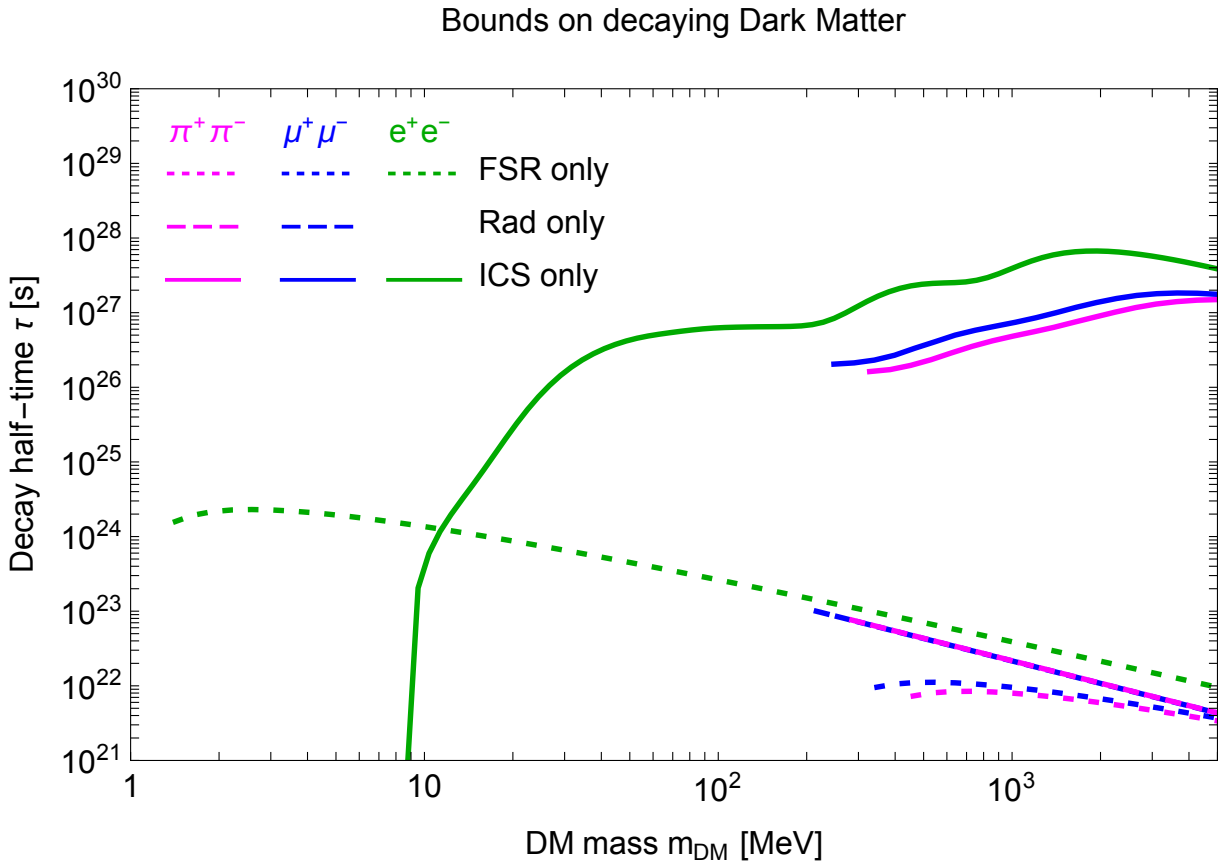

Analysis and results

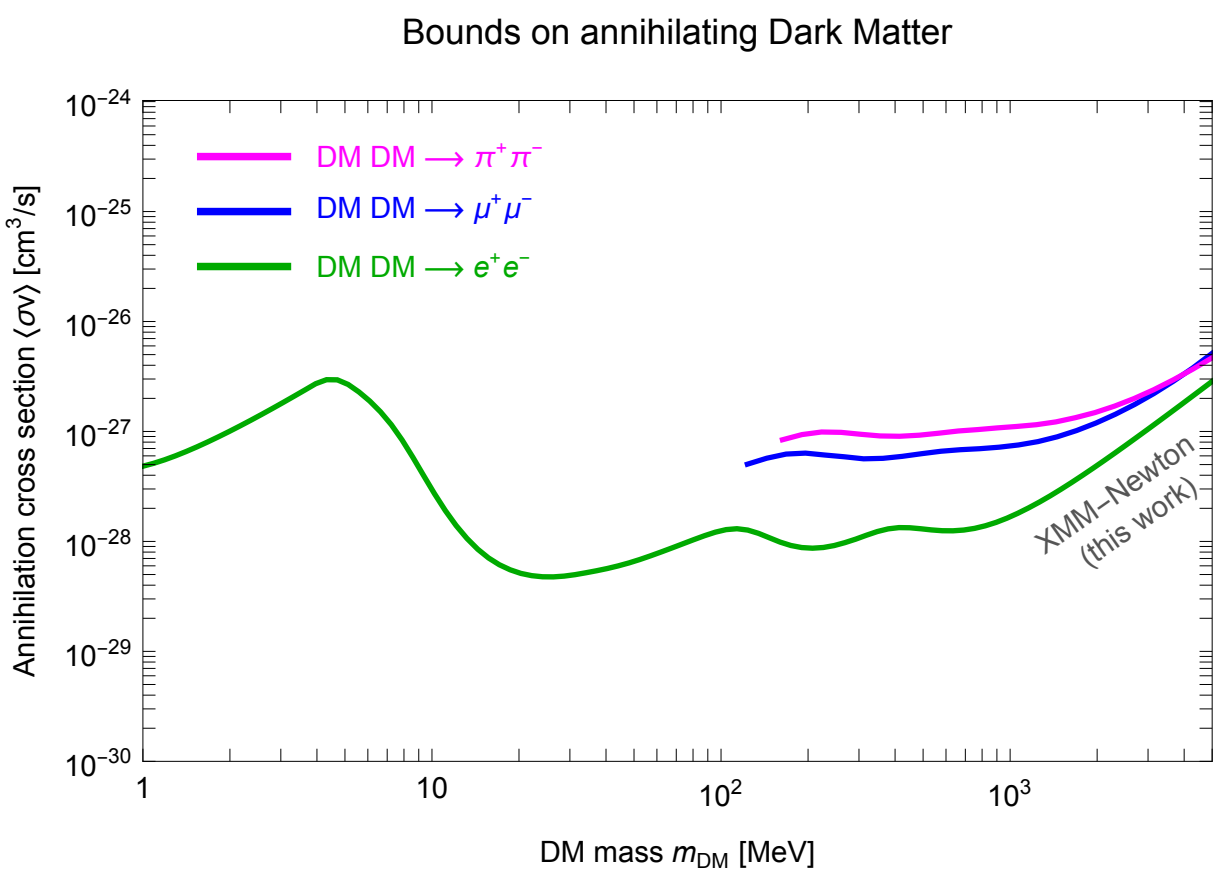

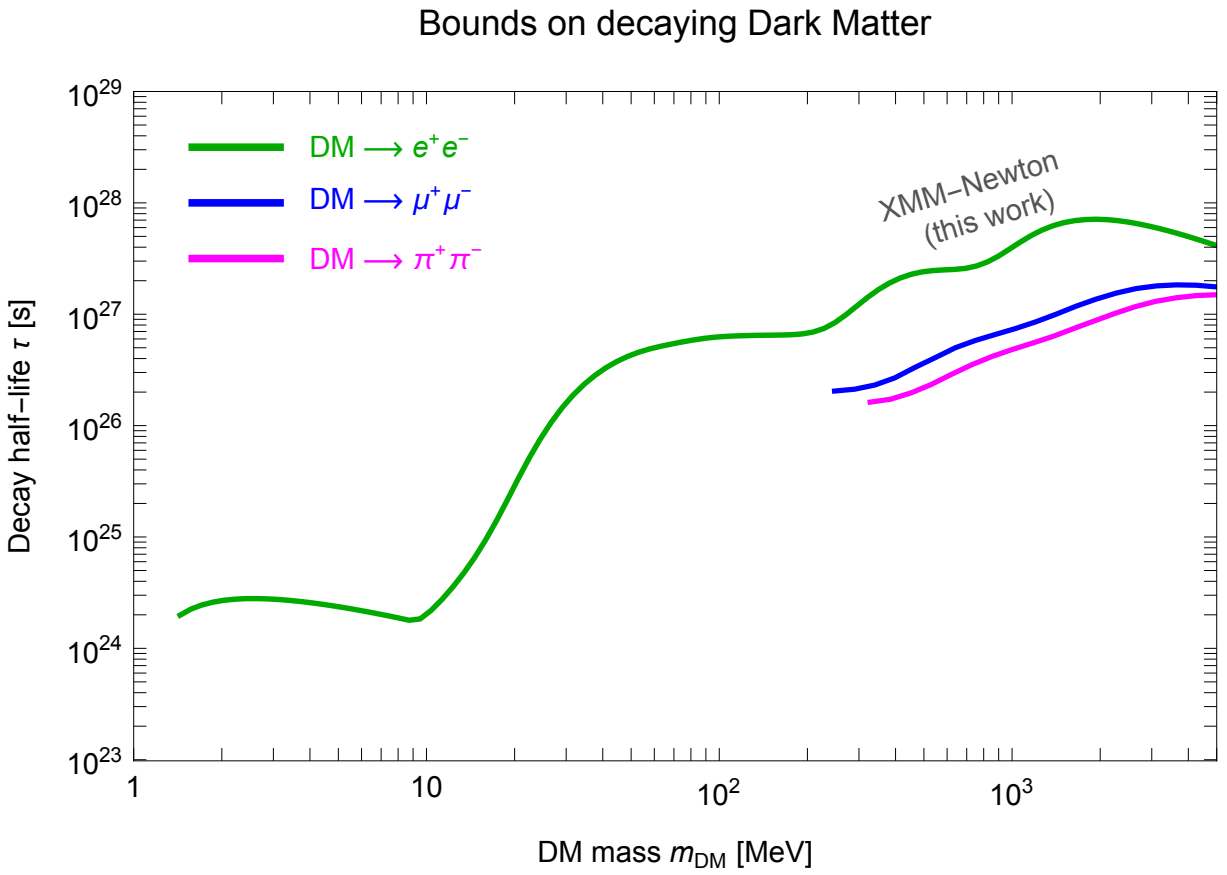

Analysis and results

Diffuse γ-rays: Essig et al., 1309.4091
Voyager1: Boudaud et al., 1612.07698
Leo T gas heating: Wakedar and Wang, 2111.08025
CMB (s-wave): Slatyer, 1506.03811,
Lopez-Honorez et al., 1303.5094,
Liu et al., 1604.02457
INTEGRAL FSR: Calore et al. 2209.06299

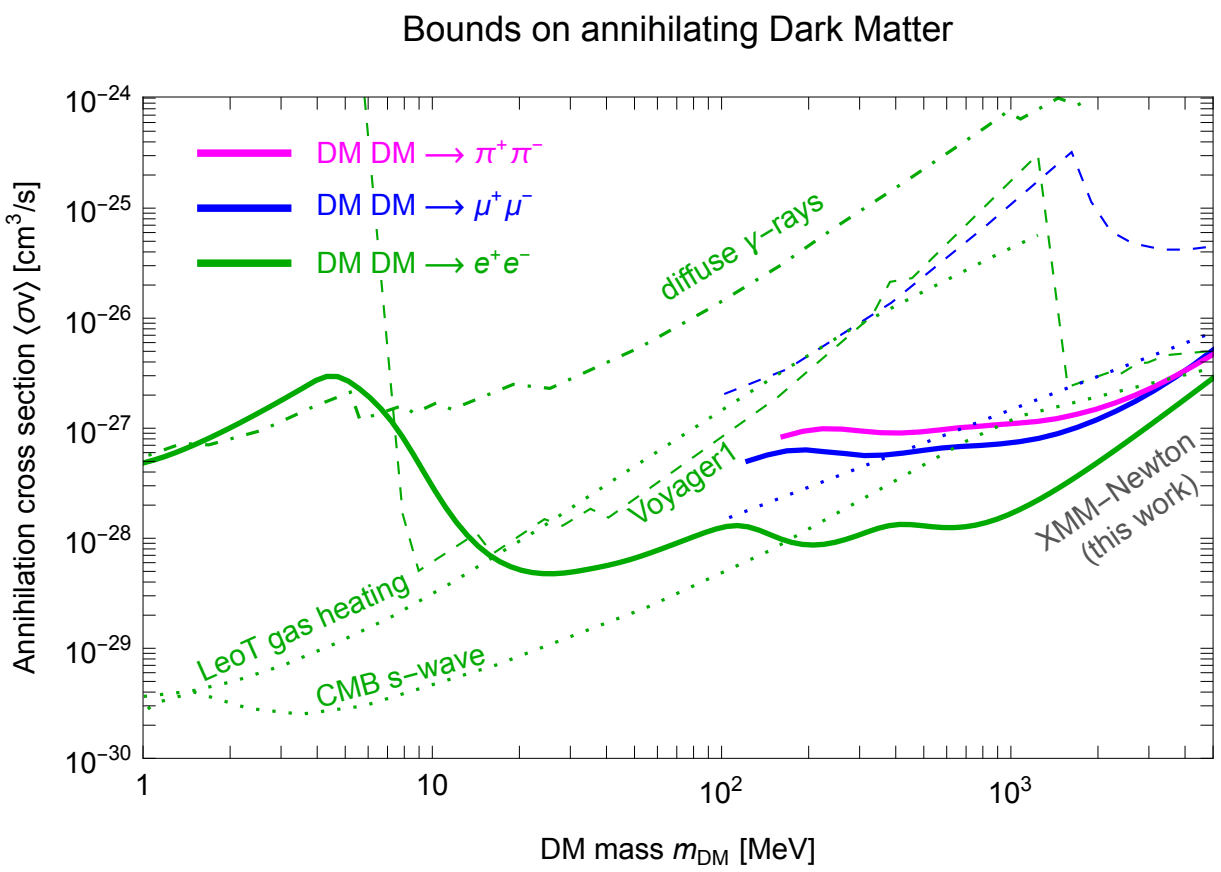

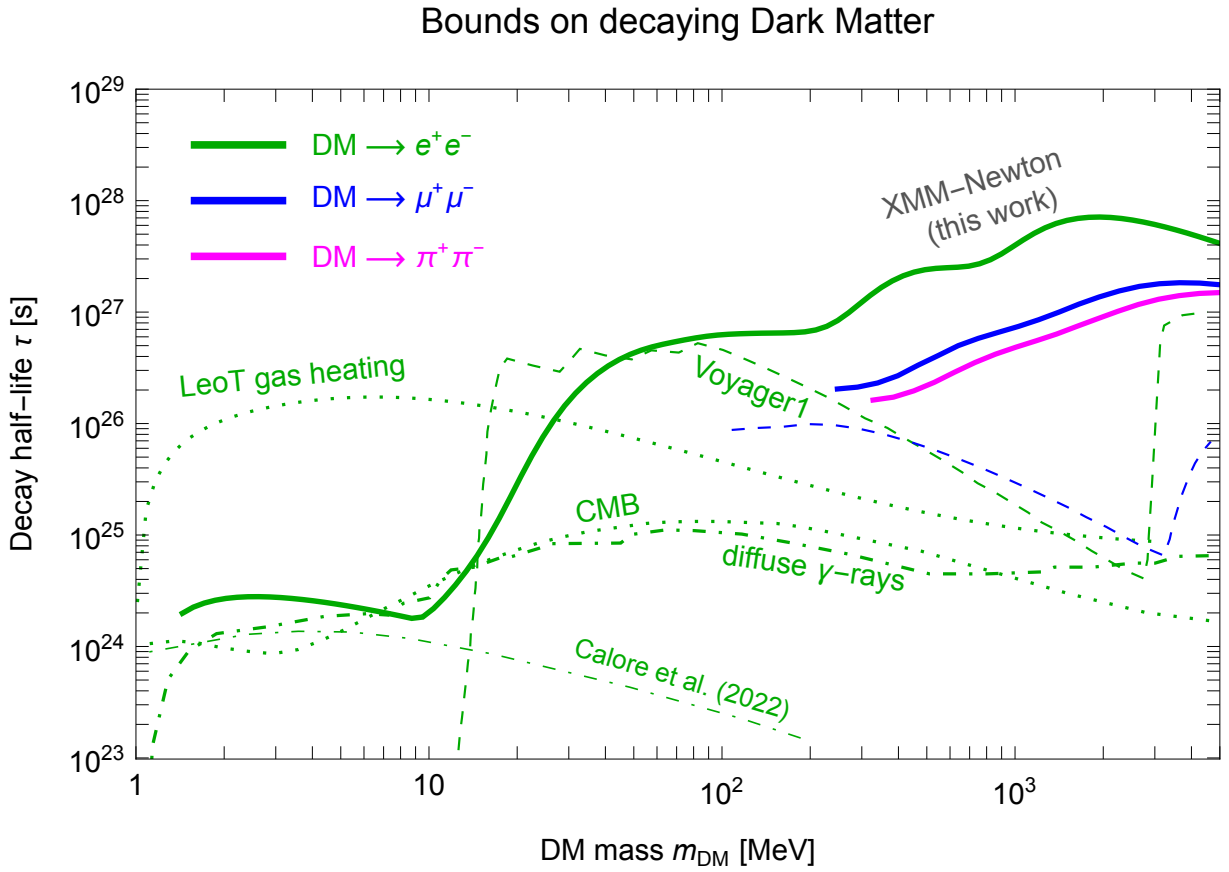

Analysis and results

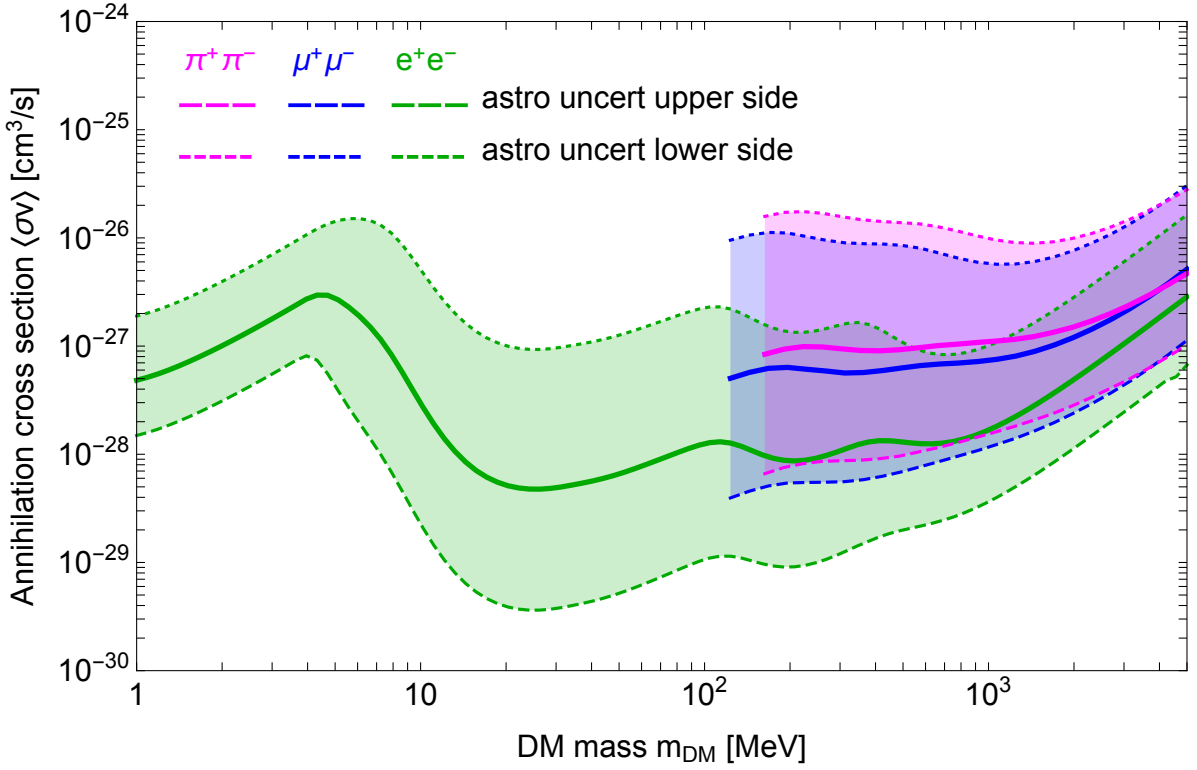

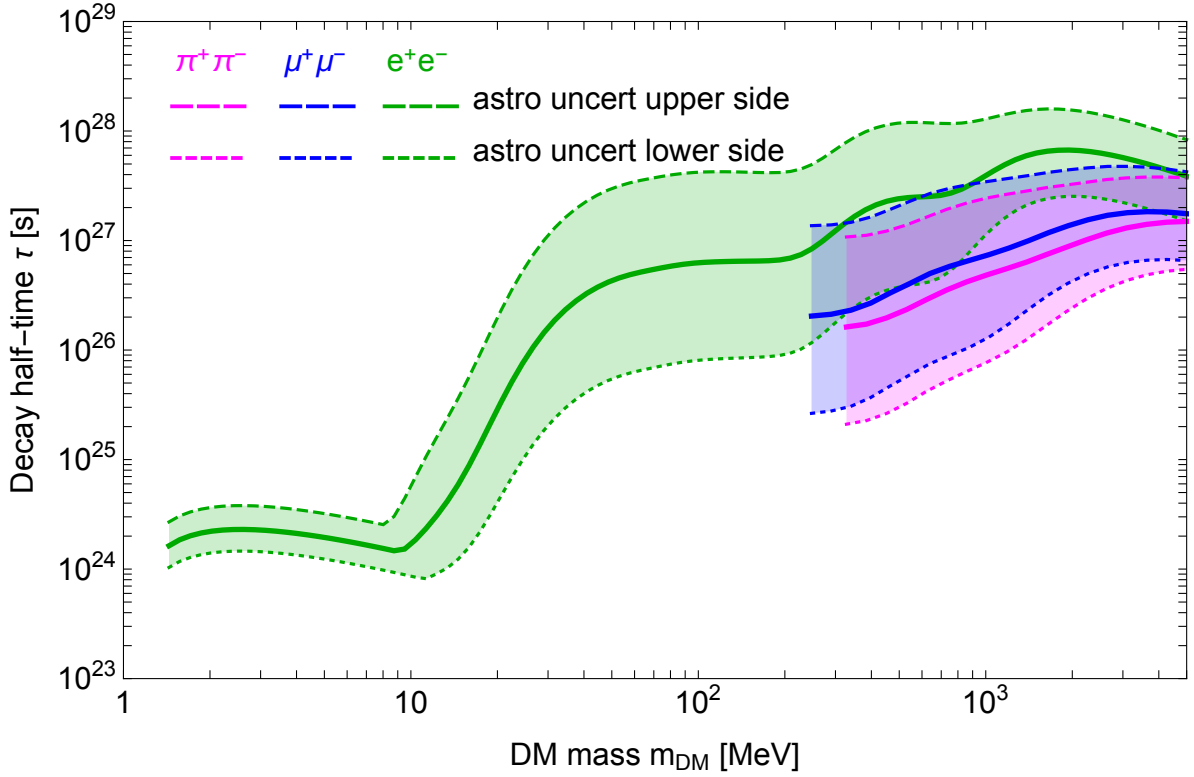

Summary

Summary

- Using secondary emission flux computations, we can compute strong bounds on light DM, while circumventing the MeV gap

Summary

- Using secondary emission flux computations, we can compute strong bounds on light DM, while circumventing the MeV gap

- Background modeling?

Summary

- Using secondary emission flux computations, we can compute strong bounds on light DM, while circumventing the MeV gap
- Background modeling?
- Theoretical uncertainties can span up to two orders of magnitudes

Thank you for your attention!

Backup

Inverse-Compton scattering

1) Local number density of ISRF photons:

- For CMB, we derive using Planck's law
- For IR and SL, we use GalPROP intensity maps, in turn based on actual observations from COBE/DIRBE

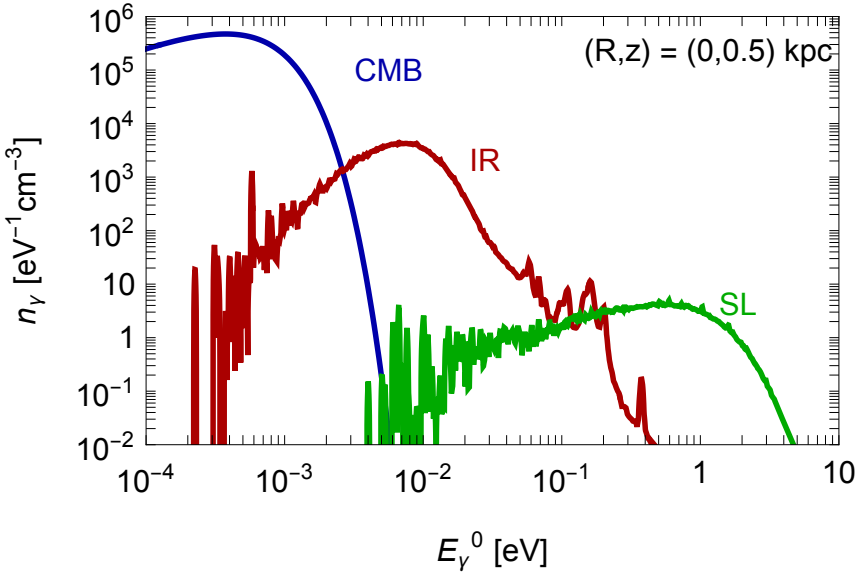

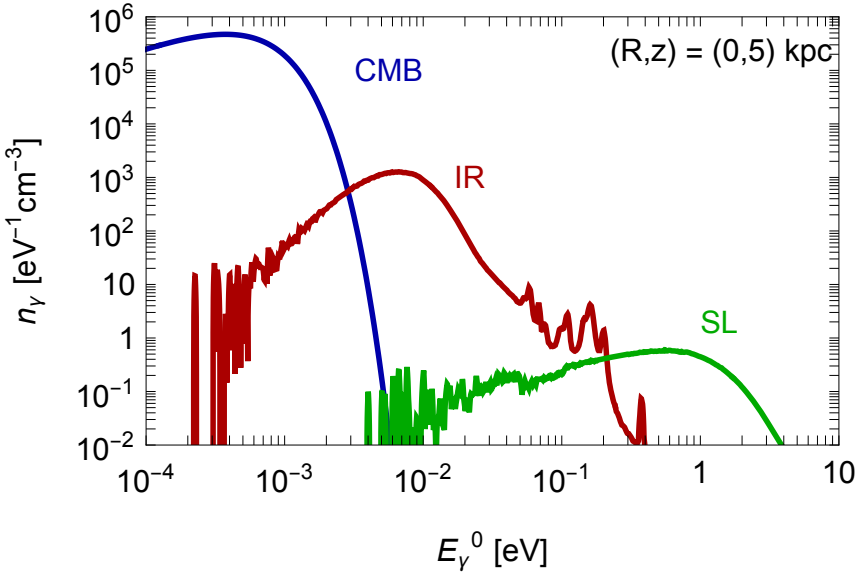

Inverse-Compton scattering

2) Local number density of DM produced $e^{\pm}$:

$$\cancel{\frac{\partial f}{\partial t}} = \cancel{\nabla(\mathcal{K}(E_e, \vec{x})\nabla f)} + \frac{\partial}{\partial E_e}(b(E_e, \vec{x})f) + Q(E_e, \vec{x})$$

diffusion term | energy loss term | source term

- We study the stationary regime
- For high-energy $e^{\pm}$ in the Milky Way, energy loss dominate over diffusion

Inverse-Compton scattering

Depends on the local ISRF density

$$b(E_e, \vec{x}) = b_{Coul+ioniz} + b_{brems} + b_{ICS} + b_{syn}$$

Depend on the local gas density

Depends on the galactic magnetic field configuration

- $b(E_e, \vec{x})$ taken from PPPC4DMID
- Diffusion curve: $b_{diff}(E_e) \sim E_e/\tau_{diff}(E_e)$

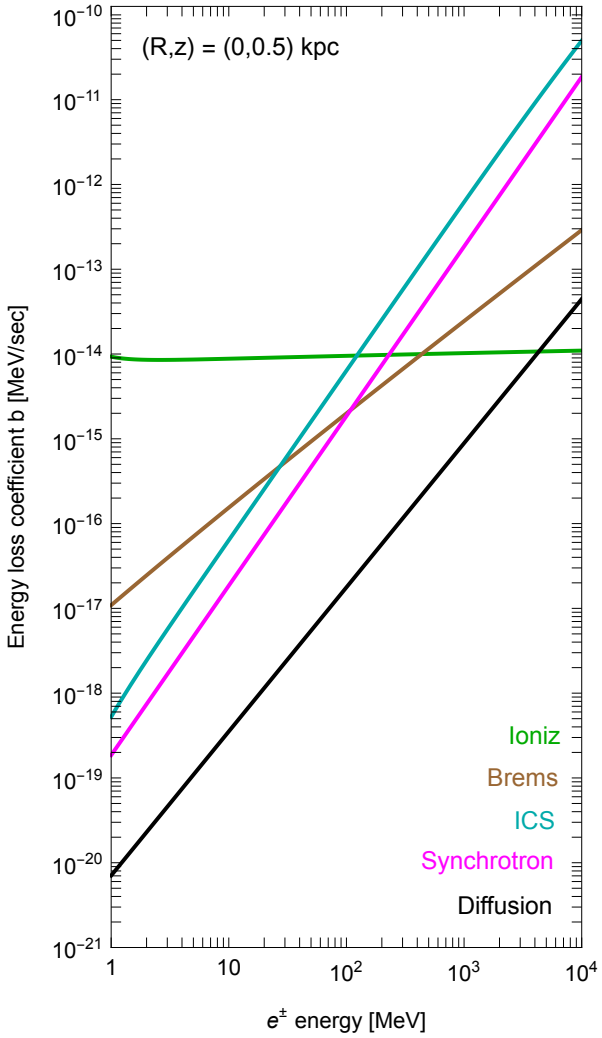

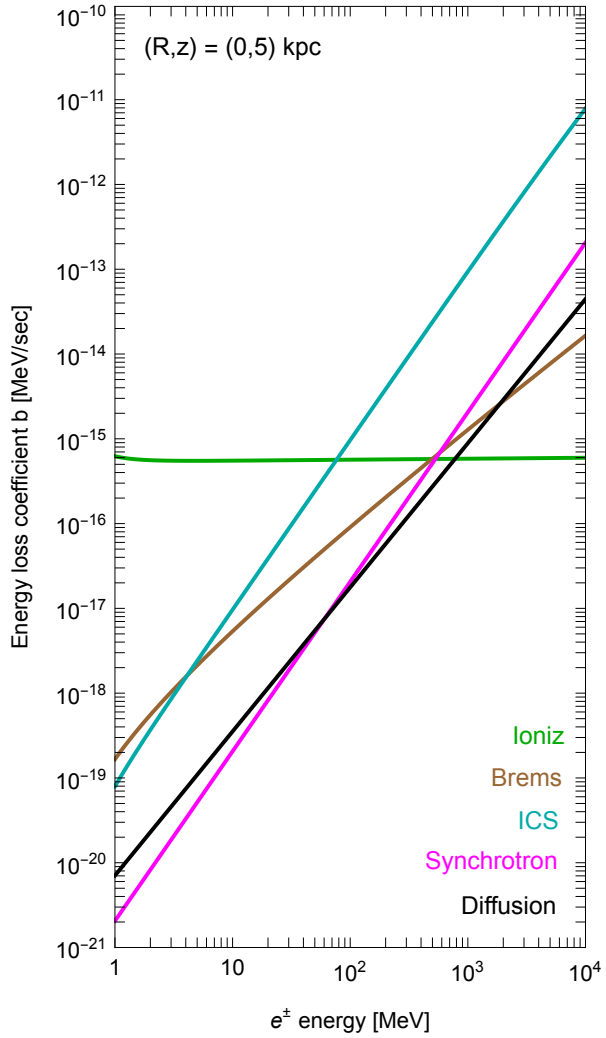

Inverse-Compton scattering

- Source term: $Q(E_e, \vec{x}) = \begin{cases} \frac{\langle \sigma v \rangle}{2} \left(\frac{\rho_{DM}(\vec{x})}{m_{DM}} \right)^2 \frac{dN_{e^\pm}}{dE_e} \\ \Gamma \left(\frac{\rho_{DM}(\vec{x})}{m_{DM}} \right) \frac{dN_{e^\pm}}{dE_e} \end{cases}$

- Where $\frac{dN_{e^\pm}}{dE_e}$ is the $e^\pm$ injection spectrum:
  - For the e^+e^- channel: monochromatic (DM $\rightarrow e^\pm$)
  - For the $\mu^+\mu^-$ channel: boosted Michel spectrum (DM $\rightarrow \mu^\pm \rightarrow e^\pm$)
  - For the $\pi^+\pi^-$ channel: double boosted Michel spectrum (DM $\rightarrow \pi^\pm \rightarrow \mu^\pm \rightarrow e^\pm$)

Michel spectrum and boosts

- Michel spectrum: $\frac{dN_e^{\mu\to e\nu\bar{\nu}}}{dE_e} = \frac{4\sqrt{\xi^2 - 4\varrho^2}}{m_\mu}[\xi(3-2\xi) + \varrho^2(3\xi - 4)]$

$$\xi = \frac{2E_e}{m_\mu}, \qquad \varrho = \frac{m_e}{m_\mu}$$

- Lorentz boost: $\frac{dN}{dE} = \frac{1}{2\beta\gamma}\int_{E'_{min}}^{E'_{max}} \frac{1}{p'}\frac{dN}{dE'}$ $\qquad E'_{\max|min} = \gamma(E \pm \beta p)$

$\gamma = \frac{E_A}{m_A}$ (A = parent particle)

Inverse-Compton scattering

3) Klein-Nishina cross section (in the Thomson limit: $E_\gamma^0 \ll E_e$)

$$\sigma_{IC}(y, E_e) = \frac{3\sigma_T}{4\gamma_e^2} \frac{2y \ln y + y + 1 - 2y^2}{y}$$

$$y = \frac{E_\gamma}{4\gamma_e^2 E_\gamma^0}, \qquad \gamma_e = \frac{E_e}{m_e}$$

Inverse-Compton scattering

- To compute the IC-scattered photon flux, we need a few ingredients:

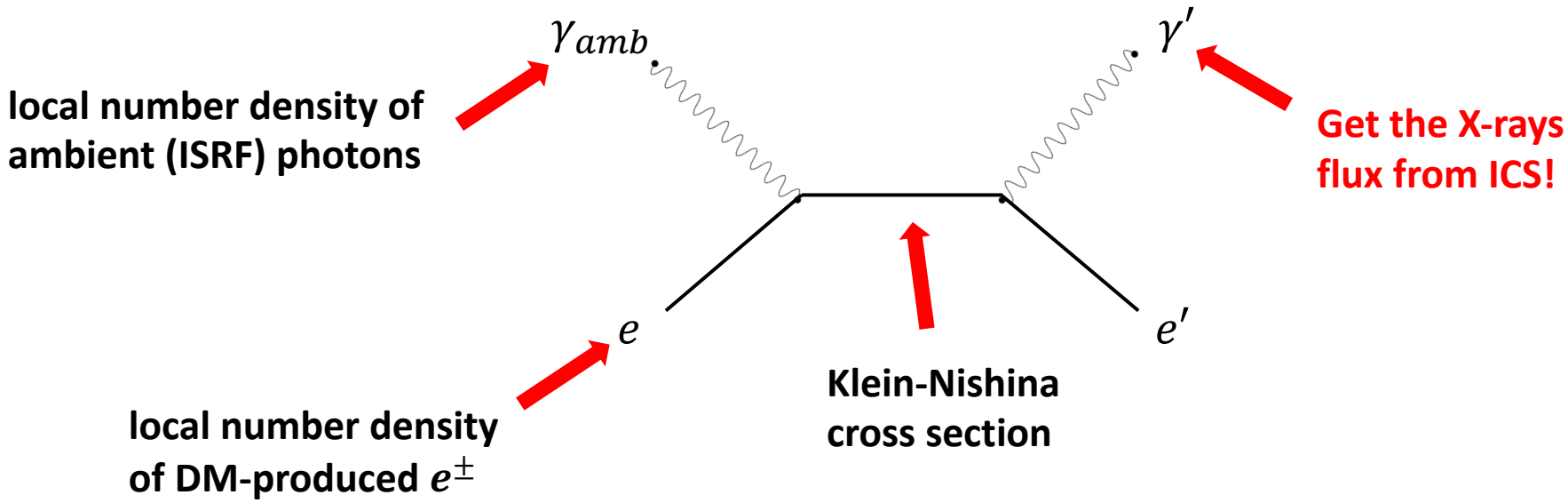

Inverse-Compton scattering

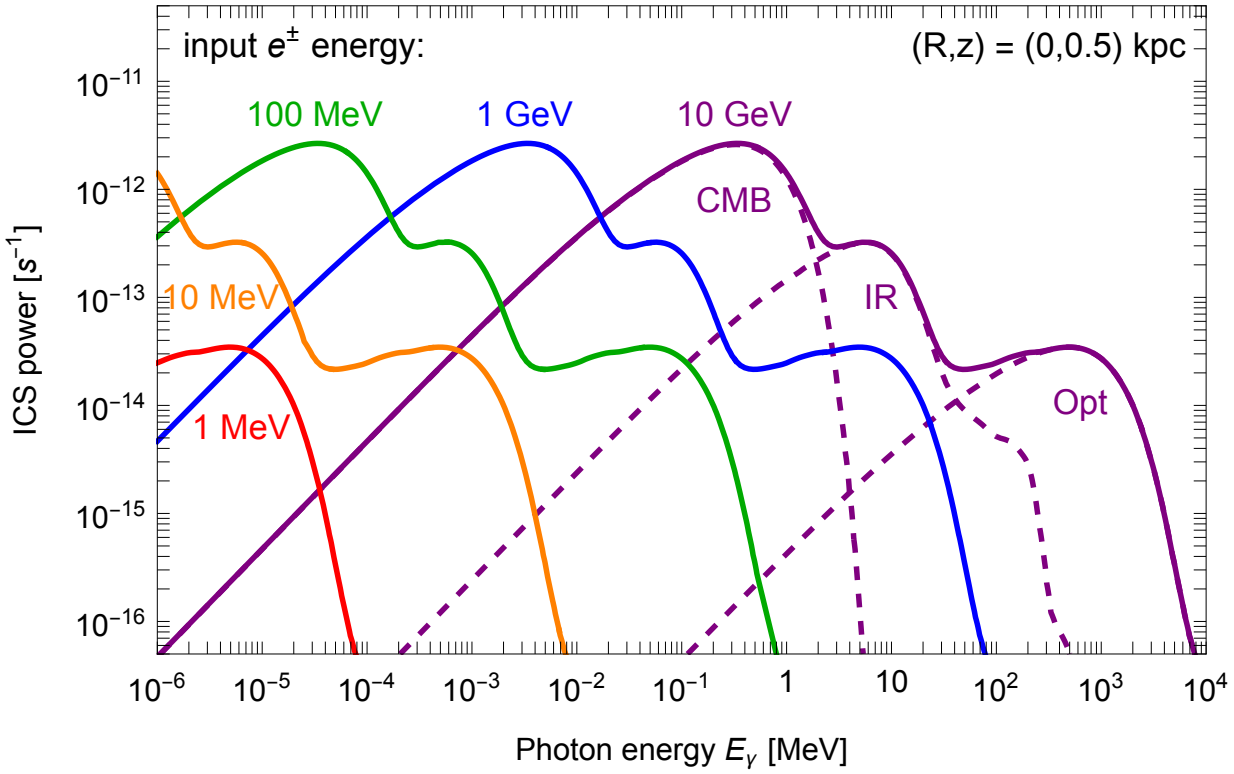

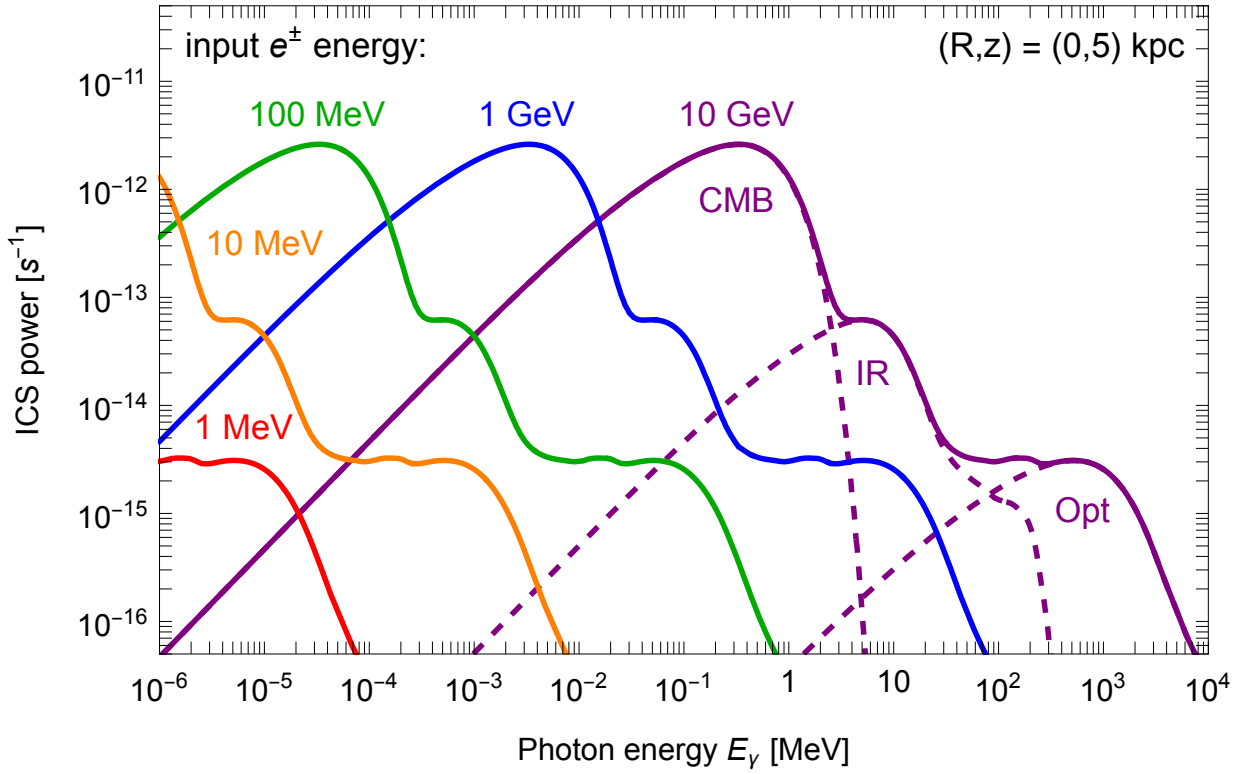

$$\mathcal{P}_{IC,i}(E_\gamma, E_e, \vec{x}) = E_\gamma \int dy\, n_i(y, \vec{x})\, \sigma_{IC}(E_e, y)$$

Inverse-Compton scattering

- To compute the IC-scattered photon flux, we need a few ingredients:

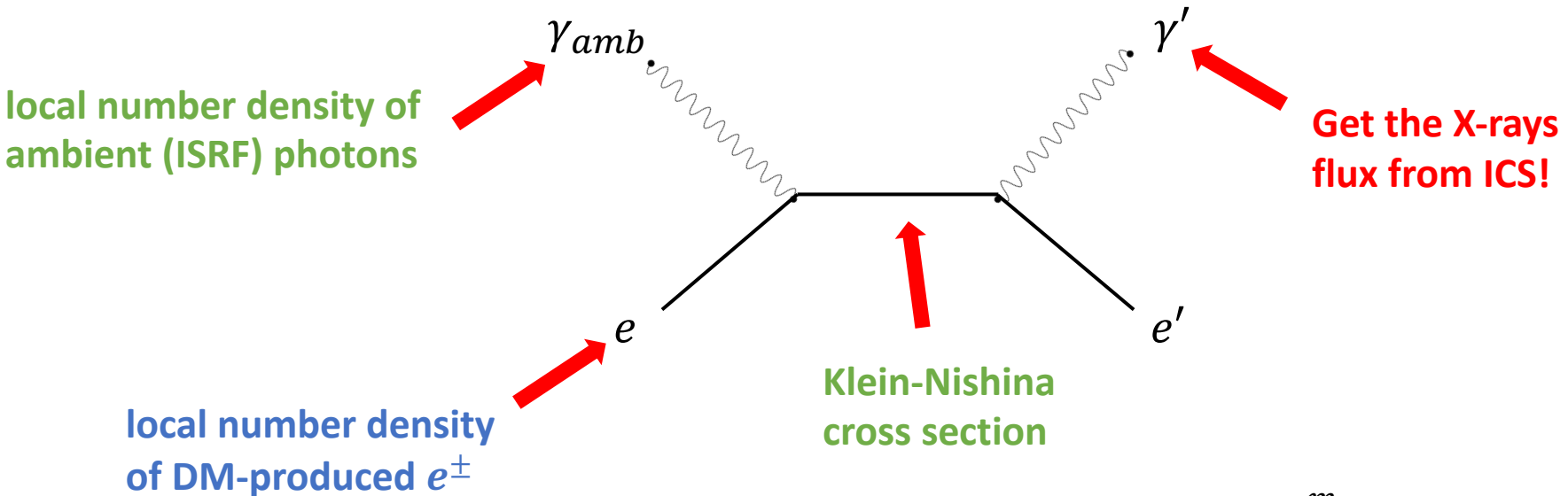

$$j(E_\gamma, \vec{x}) = 2 \int_{m_e}^{m_{DM}} dE_e \, \mathcal{P}_{IC,tot}(E_\gamma, E_e, \vec{x}) f(E_e, \vec{x})$$

Inverse-Compton scattering

- To compute the IC-scattered photon flux, we need a few ingredients:

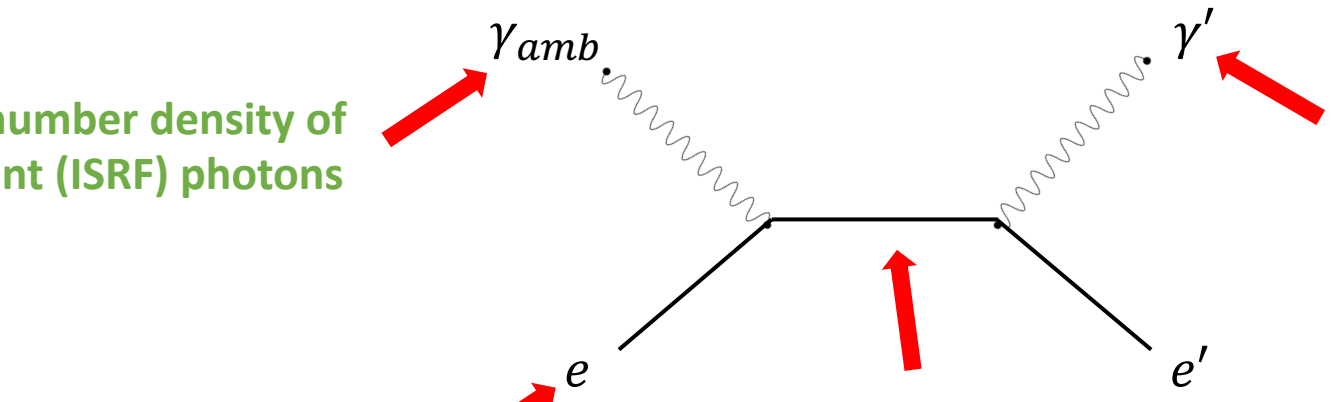

$$\frac{d\Phi_{IC\gamma}}{dE_\gamma d\Omega} = \frac{1}{4\pi E_\gamma} \int_{l.o.s.} ds\, j\left(E_\gamma, \vec{x}(s,b,l)\right)$$

Dataset energy ranges

Suzaku: 0.4 – 5 keV
XMM-Newton: 2.5 – 8 keV
NuSTAR: 3 – 20 keV
INTEGRAL: 27 – 1800 keV

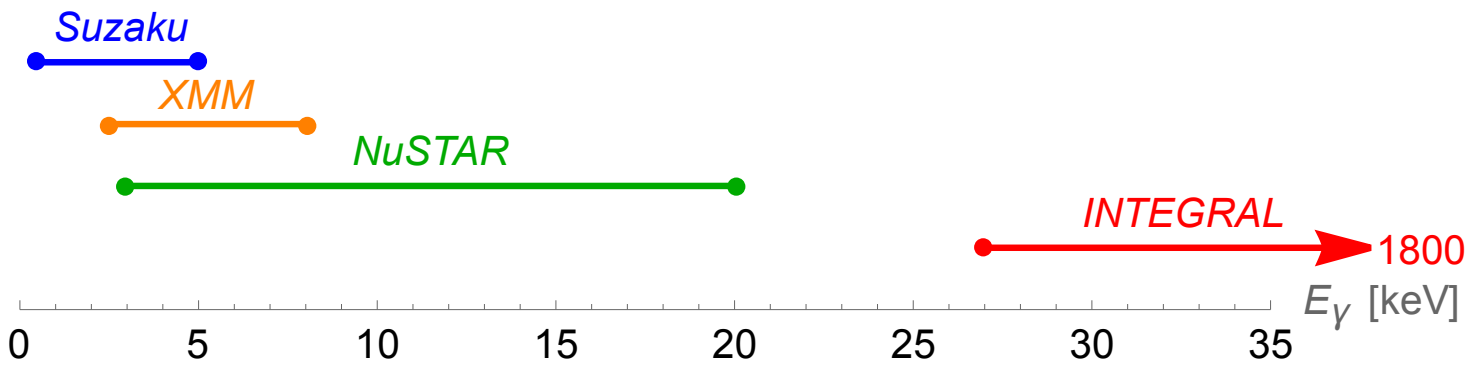

NuSTAR datasets

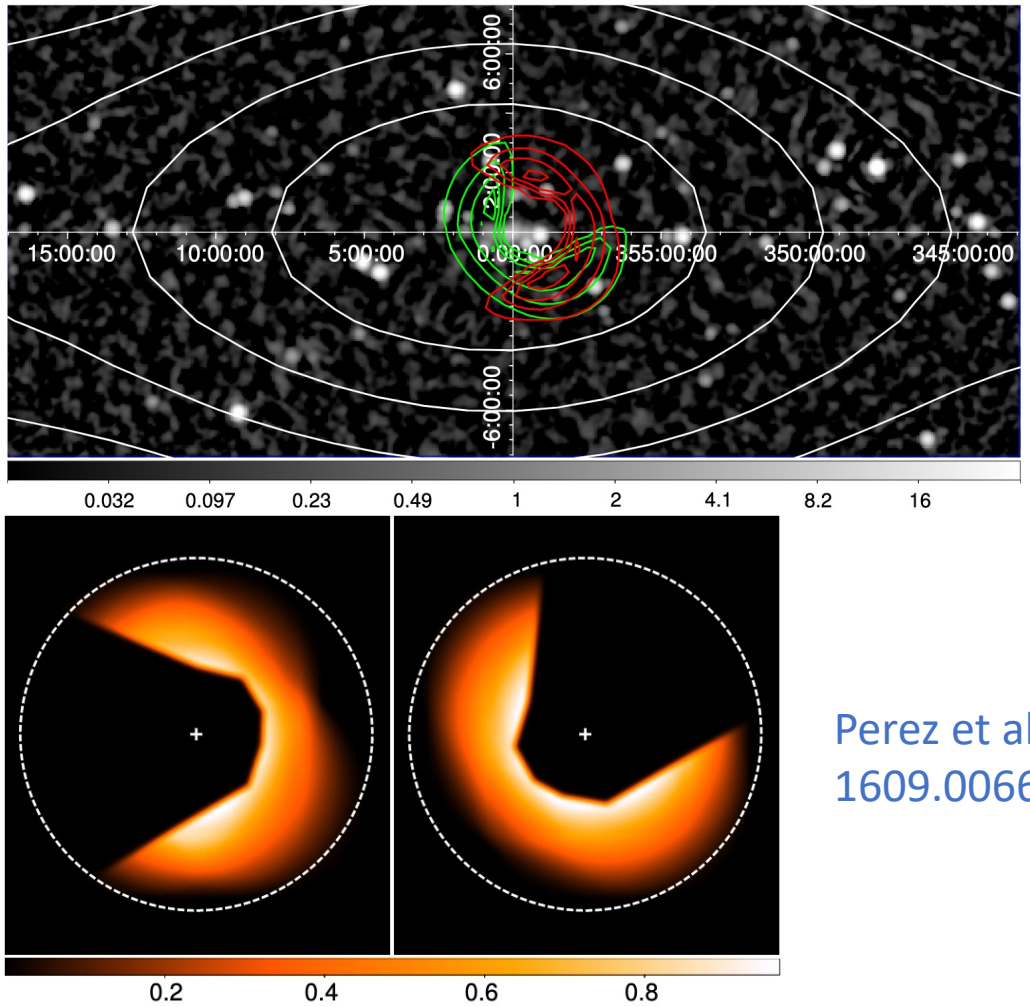

Perez et al., 1609.00667

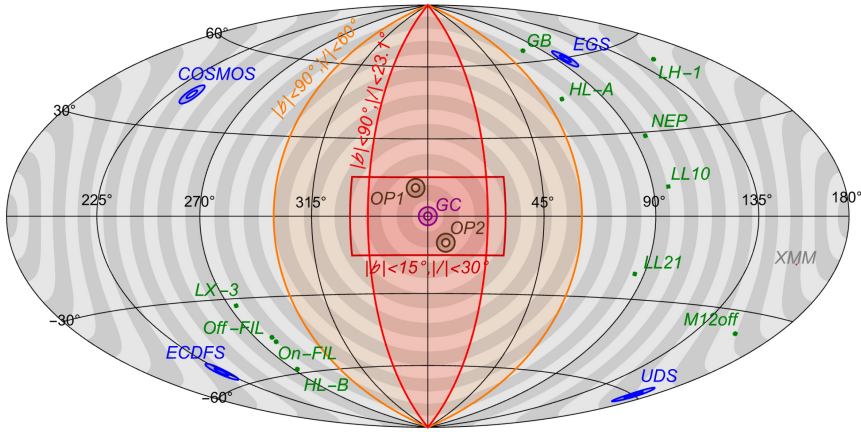

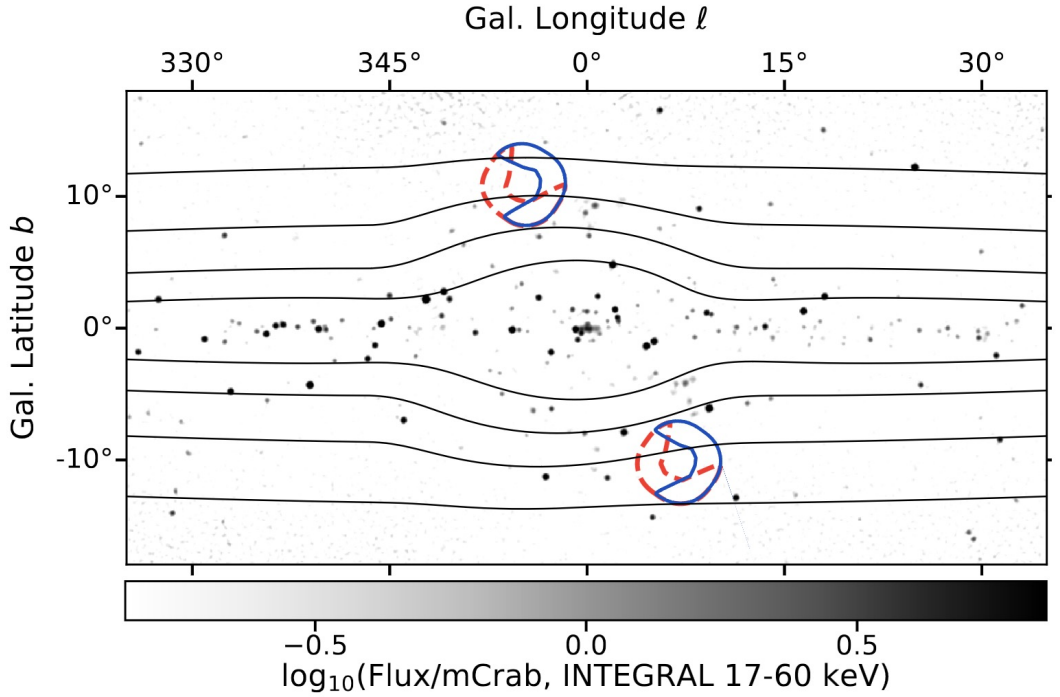

Roach et al., 1908.09037

NuSTAR datasets

Table 2. Data sets used in the analysis.

ID	Field	Begin	End	T_{exp}
1	COSMOS *EP1*	26-12-2012	20-01-2013	750 ks
2	COSMOS *EP2*	03-04-2013	21-05-2013	630 ks
3	COSMOS *EP3*	03-12-2013	25-02-2014	1020 ks
4	EGS	15-11-2013	27-11-2014	1.5 Ms
5	ECDFS	28-09-2012	01-04-2013	1.4 Ms
6	UDS	24-01-2016	18-11-2016	1.7 Ms

Krivonos et al., 2011.11469
Data taken between 2012 and 2016

TABLE I. *NuSTAR* observations used for this analysis.

Observation ID	Pointing (J2000)[a] RA (deg)	DEC (deg)	Effective Exposure[b] FPMA / FPMB (ks)	Detector Area[c] FPMA / FPMB (cm^2)	Avg. Solid Angle[d] FPMA / FPMB (deg^2)
40032001002	265.8947	−29.5664	39.7 / 39.6	9.89 / 11.10	3.73 / 4.09
40032002001	265.7969	−29.5139	39.8 / 39.6	7.14 / 8.05	4.06 / 4.12
40032003001	265.6991	−29.4613	39.8 / 39.6	8.18 / 8.92	3.47 / 4.01
40032004002	265.9550	−29.4812	22.6 / 22.7	4.19 / 6.54	2.34 / 3.13
40032005002	265.8572	−29.4288	25.6 / 25.8	9.78 / 7.85	3.80 / 3.85
40032006001	265.7595	−29.3762	28.6 / 28.6	9.98 / 6.18	3.76 / 3.74

[a] Roll angle was 332° for all.
[b] After all data cleaning.
[c] After stray light, ghost ray, and bad pixel removal.
[d] Average solid angle of sky from which 0-bounce photons can be detected, after correcting for removal of stray light, ghost rays, and bad pixels, as well as efficiency due to vignetting effects.

Perez et al., 1609.00667
Data taken between 2012 and 2014

TABLE I. NuSTAR Galactic Bulge observations used in this analysis, with 0-bounce effective areas after data cleaning.

NuSTAR obsID	Pointing (J2000) RA, Dec (deg)	Effective Exposure[a] FPMA / B (ks)	Detector Area A_{0b}[b] FPMA / B (cm^2)	Solid Angle $\Delta\Omega_{0b}$[c] FPMA / B (deg^2)
40410001002	253.2508, -26.6472	50.0 / 49.8	11.97 / 11.88	4.36 / 4.62
40410002002	280.3521, -27.6344	44.7 / 44.6	12.71 / 12.60	4.53 / 4.56

[a] After `OPTIMIZED` SAA filtering and manual data screening.
[b] After bad pixel removal (both obsIDs) and point-source masking (40410001002 only).
[c] Average solid angle of sky for detecting 0-bounce photons, after correcting for bad pixel removal and vignetting efficiency.

Roach et al., 1908.09037
Data taken between in 2018

NuSTAR constraints

NuSTAR (2012-2018 data):

- blank-sky fields Krivonos et al., 2011.11469
- GC obs. Perez et al., 1609.00667
- off-plane obs. Roach et al., 1908.09037

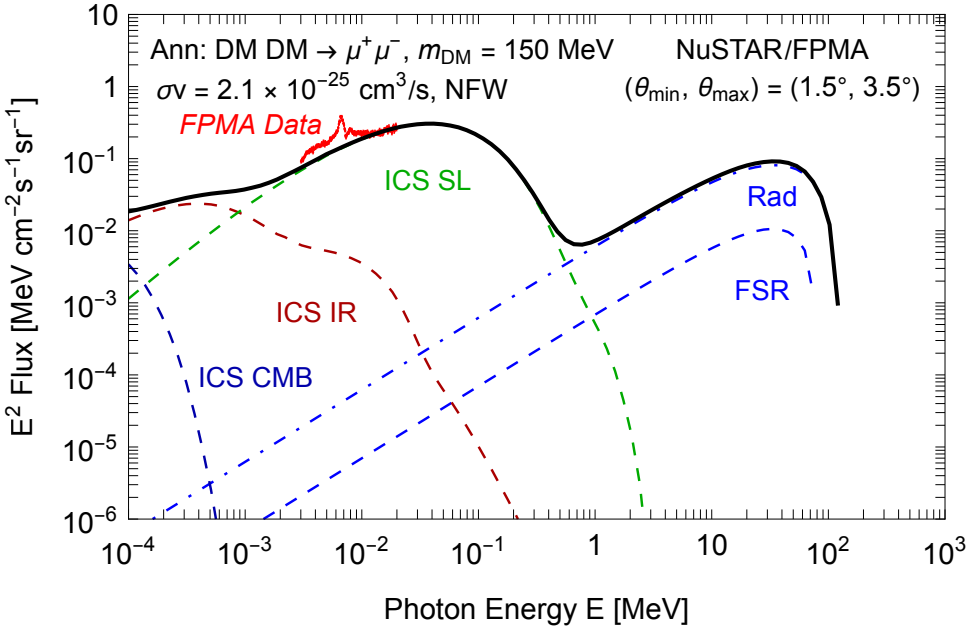

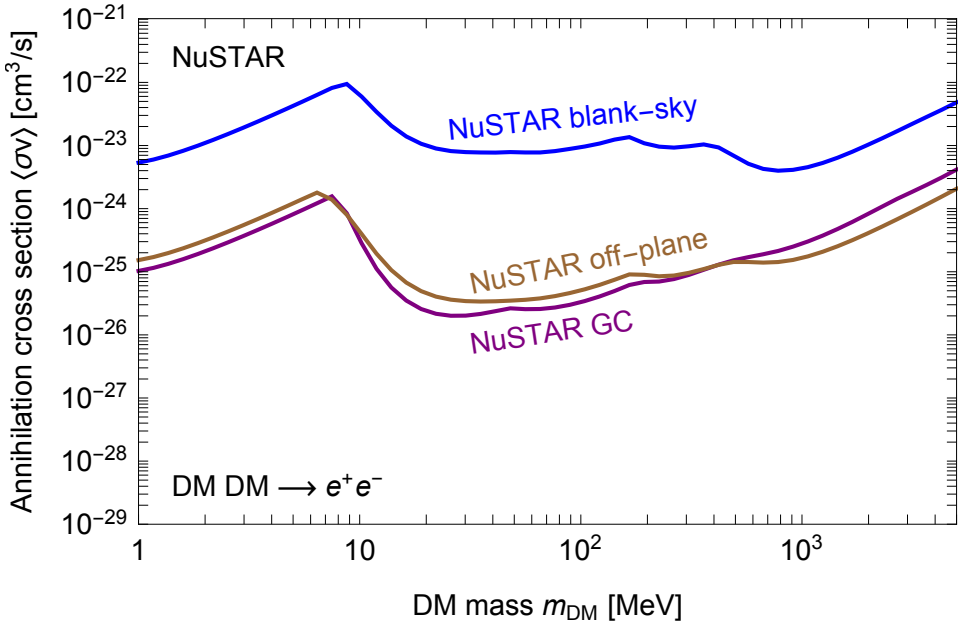

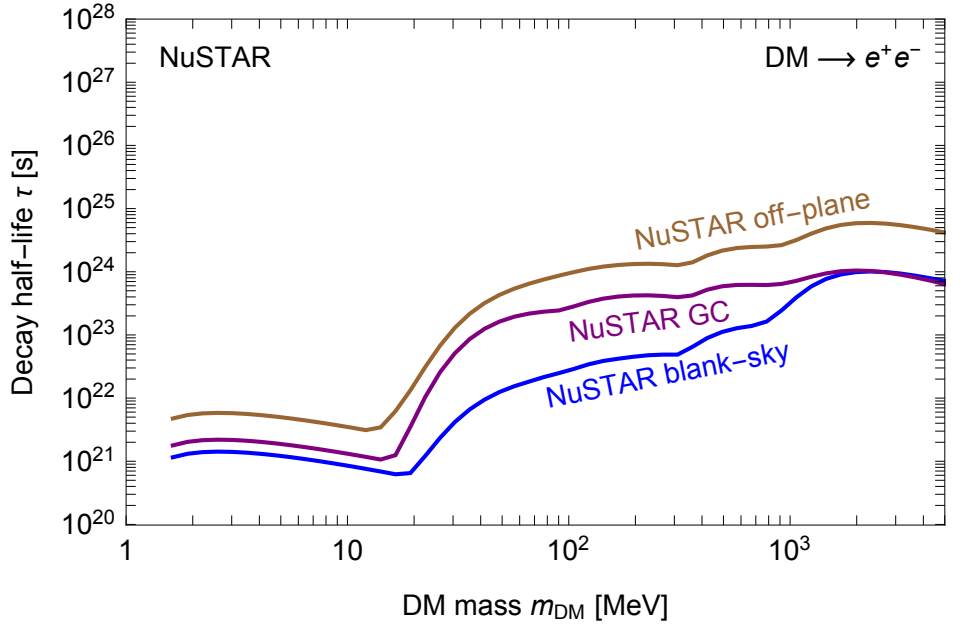

Suzaku datasets

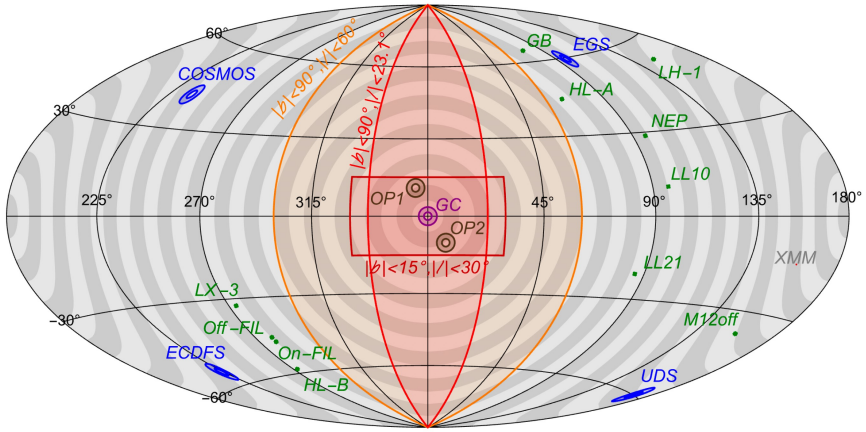

Table 1. Log of observations, ordered by $|b|$

Data set ID	Field Name (Short Name)	Obs ID	Date	Exposure (ks) Total	Cleaned	Aim point (ℓ, b)	$(E_{\rm Lon}, E_{\rm Lat})^*$
1	GB1428+4217 (GB)	701092010	Jun 12-13, 2006	48.7	34.9	(75.9, 64.9)	(194.2, 52.7)
2	High latitude B (HL-B)	500027020	Feb 17-20, 2006	103.6	29.7	(272.4, -58.3)	(4.4, -61.4)
3	Lockman hole 2 (LH-2)	101002010	May 17-19, 2006	80.4	40.0	(149.7, 53.2)	(137.1, 45.1)
4	Lockman hole 1 (LH-1)	100046010	Nov 14-15, 2005	77.0	61.7	(149.0, 53.2)	(137.2, 45.5)
5	Off Filament[a] (Off-FIL)	501001010	Mar 1-2, 2006	80.1	59.6	(278.7, -47.1)	(354.8, -72.6)
6	On Filament[a] (On-FIL)	501002010	Mar 3-6 , 2006	101.4	59.2	(278.7 , -45.3)	(354.1, -74.4)
7	High latitude A (HL-A)	500027010	Feb 14-15, 2006	73.6	53.2	(68.4, 44.4)	(228.8, 63.5)
8	MBM12 off cloud[b] (M12off)	501104010	Feb 6-8, 2006	75.3	51.0	(157.3, -36.8)	(44.5, 2.3)
9	LMC X-3 Vicinity[c] (LX-3)	500031010	Mar 17-18, 2006	82.0	56.1	(273.4, -32.6)	(41.2, -86.2)
10	North Ecliptic Pole 1[d] (NEP1)	100018010	Sep 2-4, 2005	106.2	58.7	(95.8, 28.7)	(334.8, 88.7)
11	North Ecliptic Pole 2 (NEP2)	500026010	Feb 10-12, 2006	75.6	16.5	(95.8, 28.7)	(334.8, 88.7)
12	Low latitude 86-21 (LL21)	502047010	May 9-10, 2007	81.5	57.0	(86.0, -20.8)	(347.6, 38.4)
13	Low latitude 97+10 (LL10)	503075010	Apr 15-16, 2008	79.8	40.8	(96.6, 10.4)	(0.7, 70.6)
R1	MBM12 on cloud[b,e] (M12on)	500015010	Feb 3-6, 2006	102.9	68.0	(159.2, -34.5)	(47.2, 2.6)
R2	Midplane 235[e] (MP235)	502021010	Apr 22-25, 2007	189.5	53.0	(235.0, 0.0)	(119.5, -40.6)

Results previously published by [a] Henley et al. (2007), [b] Smith et al. (2007), [c] Yao et al. (2009), [d] Fujimoto et al. (2007), [e] Masui et al. (2009).
* Ecliptic coordinate

Yoshino et al., 0903.2981

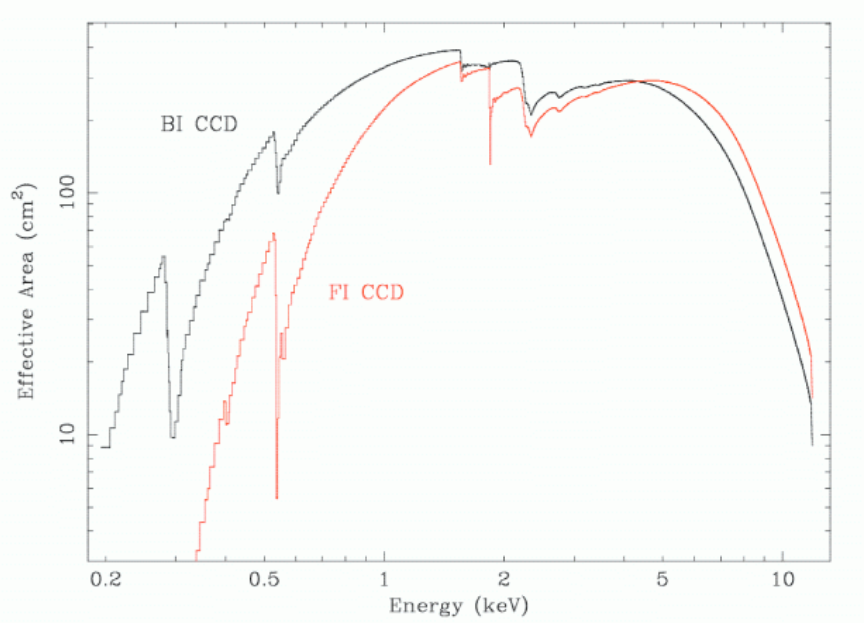

https://heasarc.gsfc.nasa.gov/docs/suzaku/gallery/performance/xis_area.html

Suzaku constraints

Suzaku high-latitude fields

2006-2008

Yoshino et al., 0903.2981

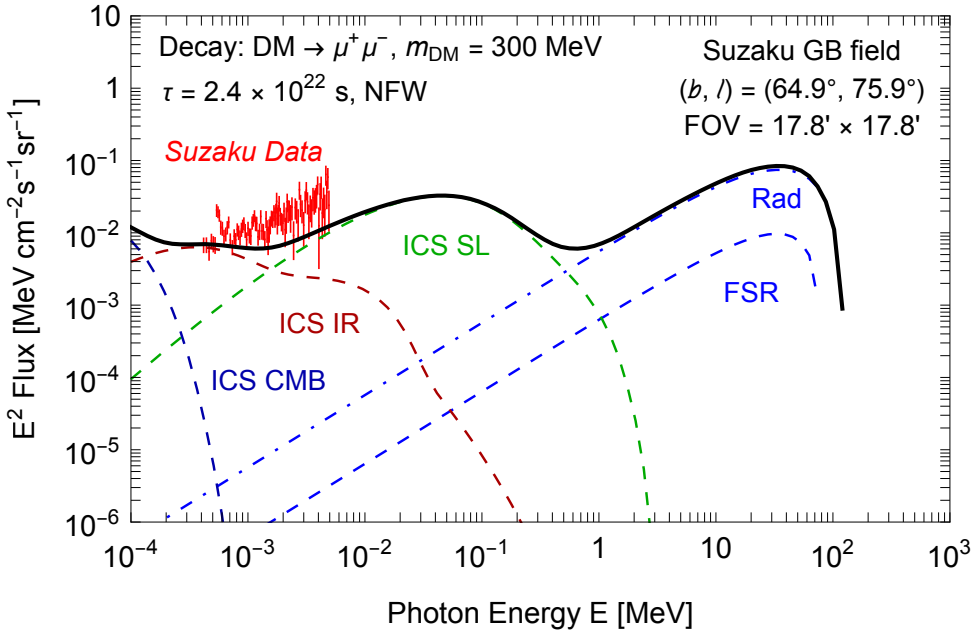

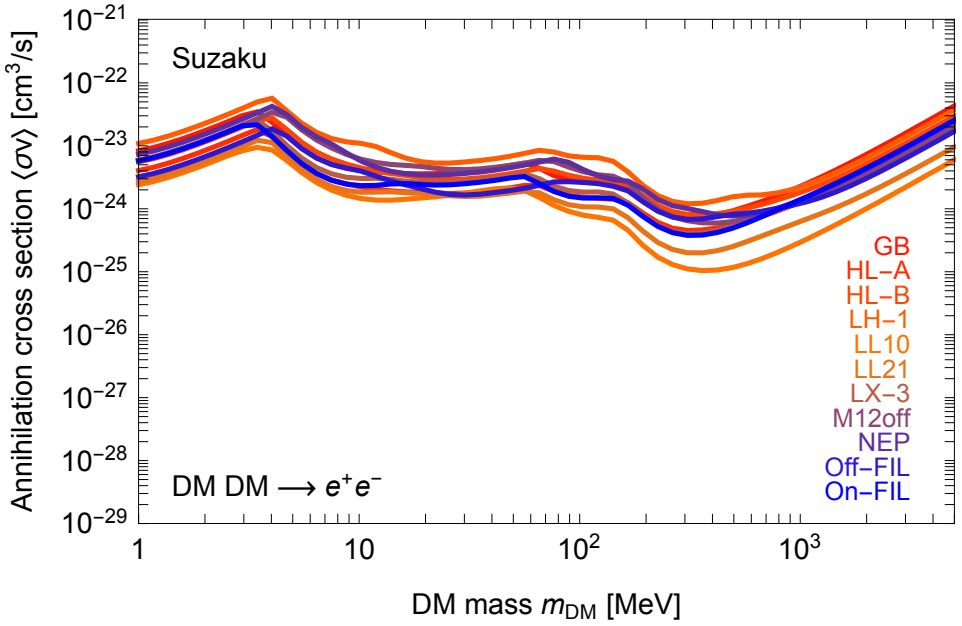

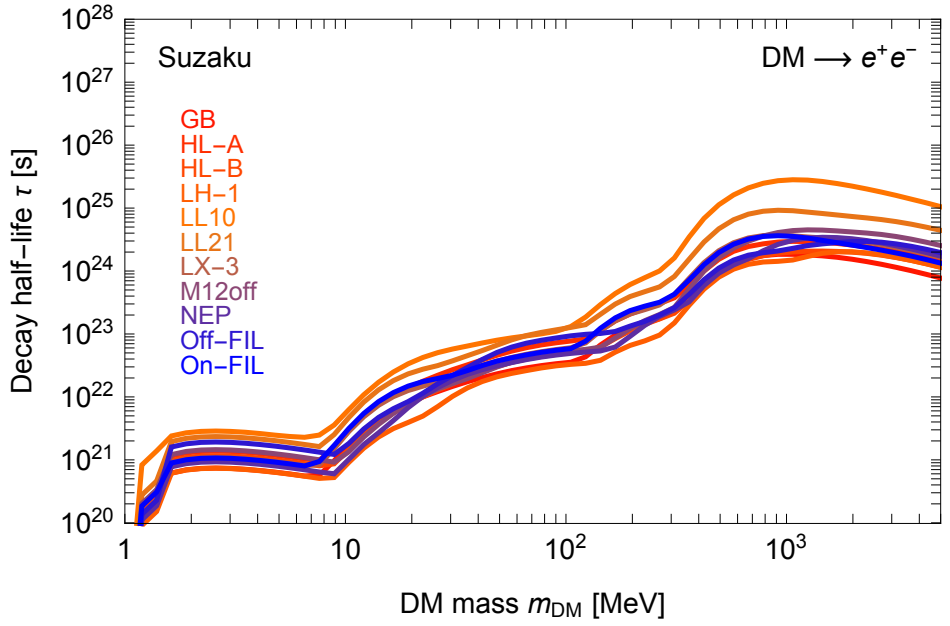

INTEGRAL datasets

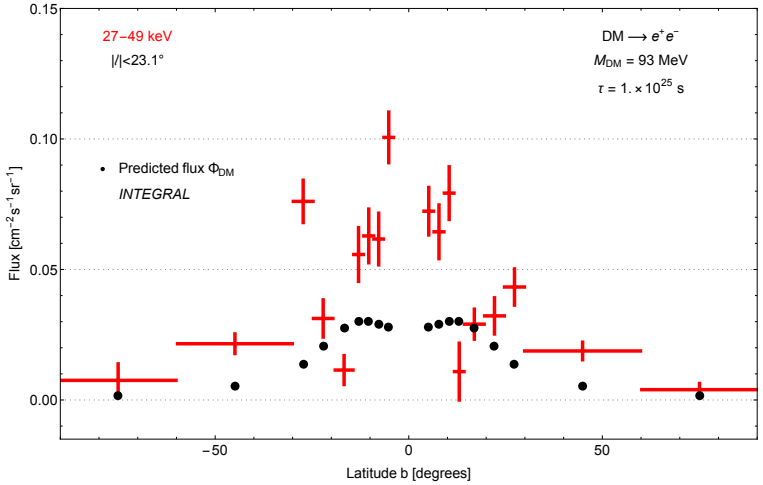

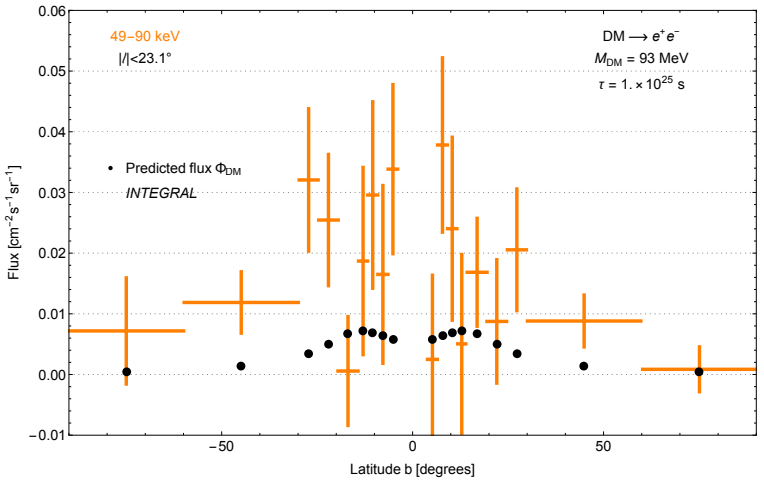

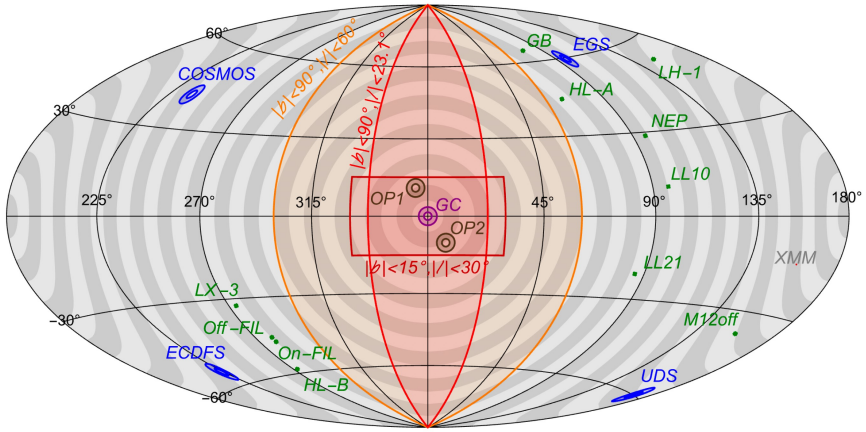

Bouchet et al., INTEGRAL coll., 1107.0200

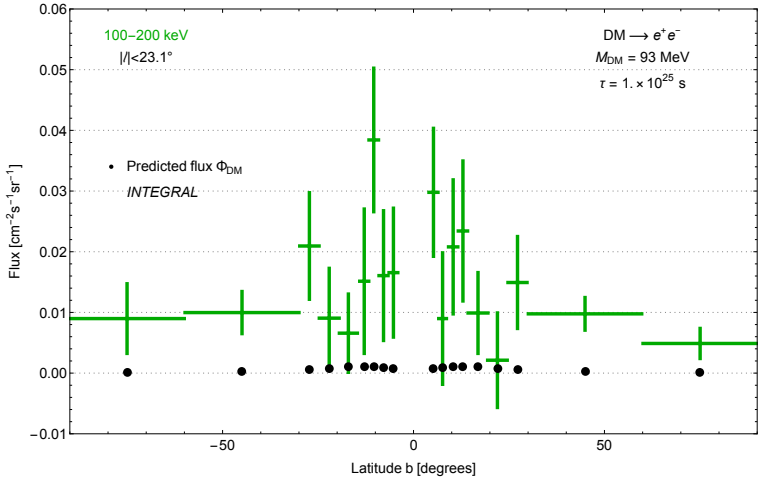

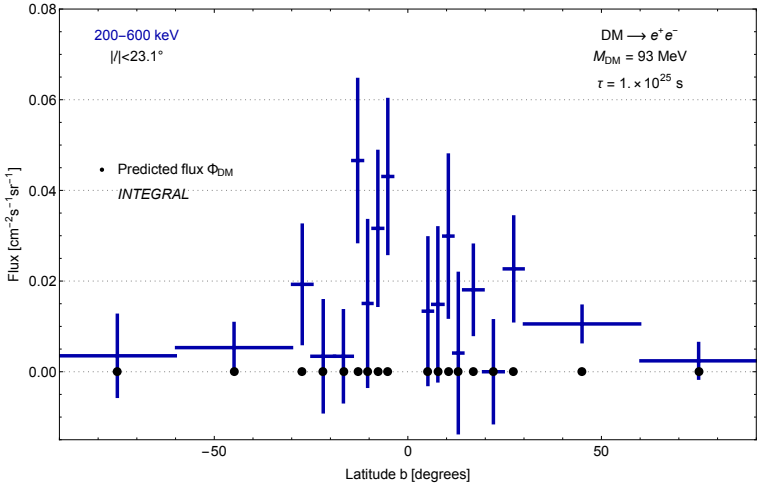

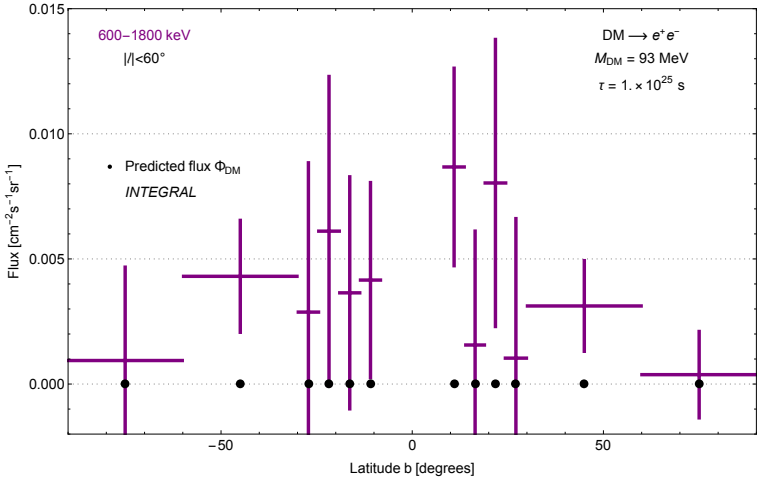

INTEGRAL constraints

INTEGRAL diffuse emission searches

2003-2009

Bouchet et al., INTEGRAL coll., 1107.0200

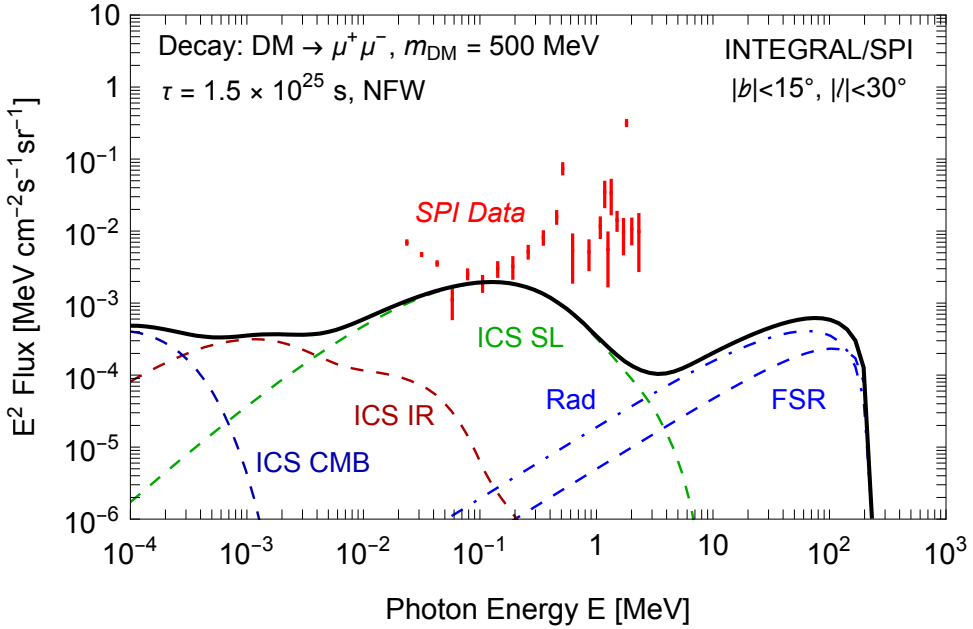

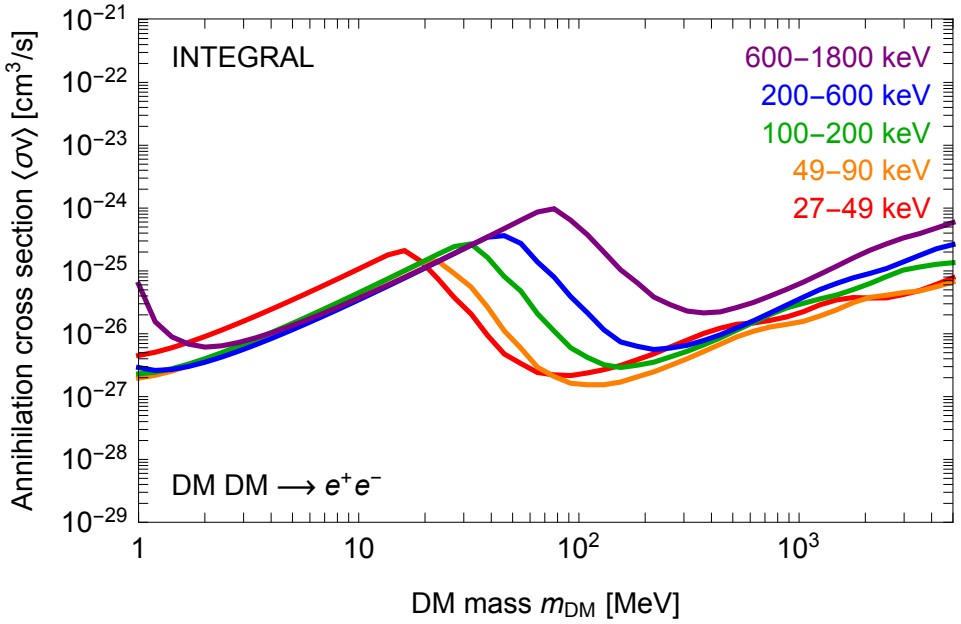

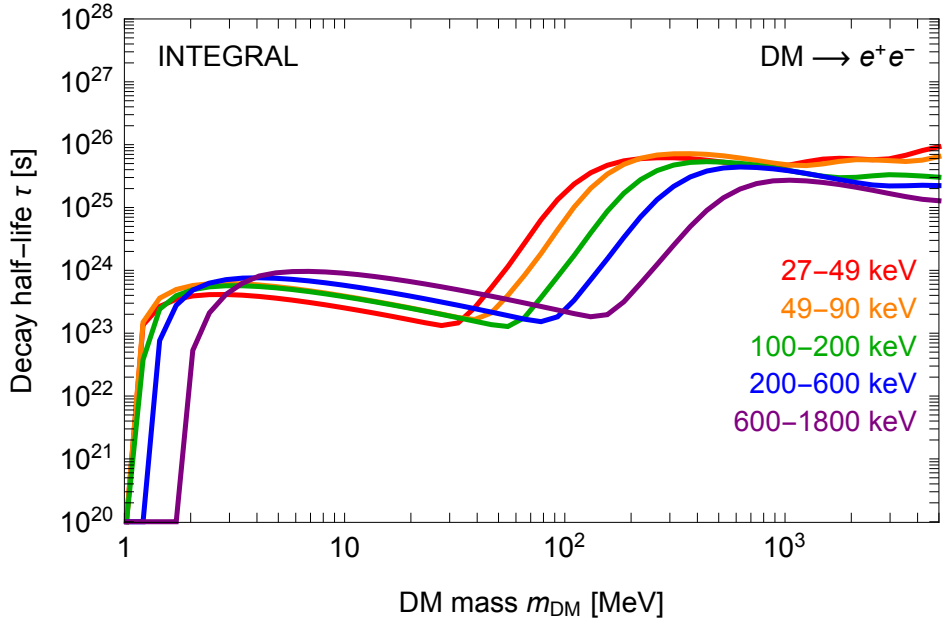

XMM-Newton datasets

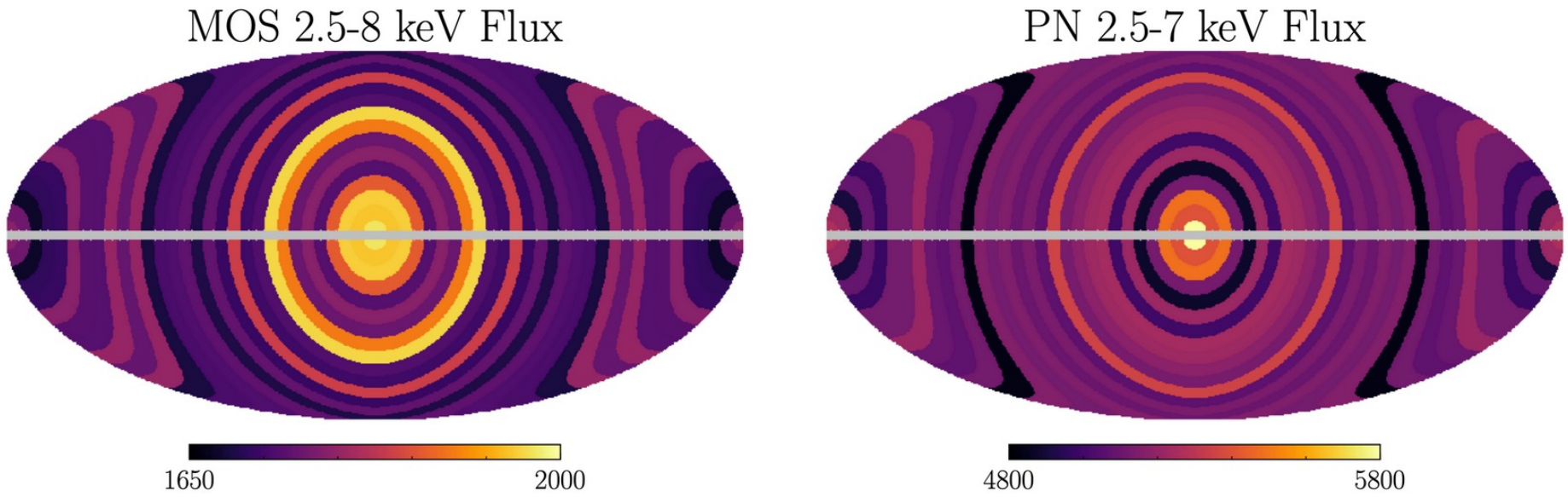

https://github.com/bsafdi/XMM_BSO_DATA

Datasets + Instrument response functions

XMM-Newton constraints

XMM-Newton whole-sky observations

1999-2018

Foster et al., 2102.02207

https://github.com/bsafdi/XMM_BSO_DATA

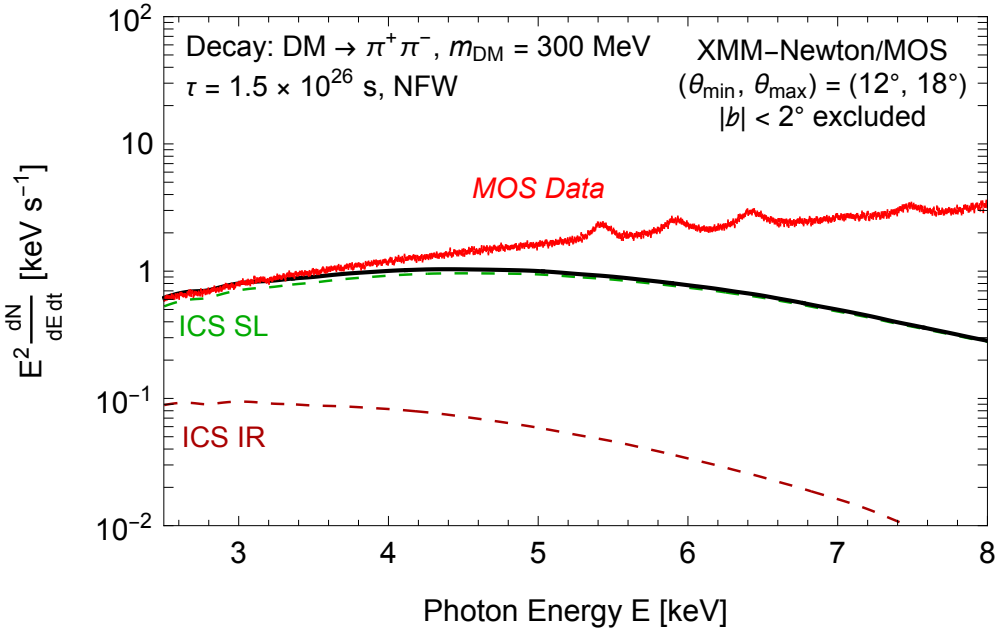

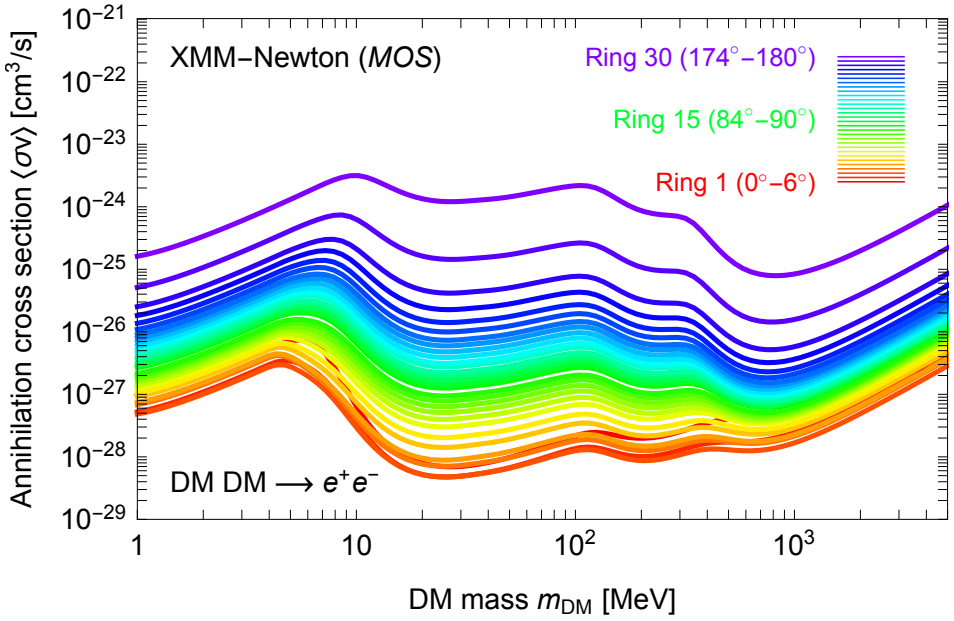

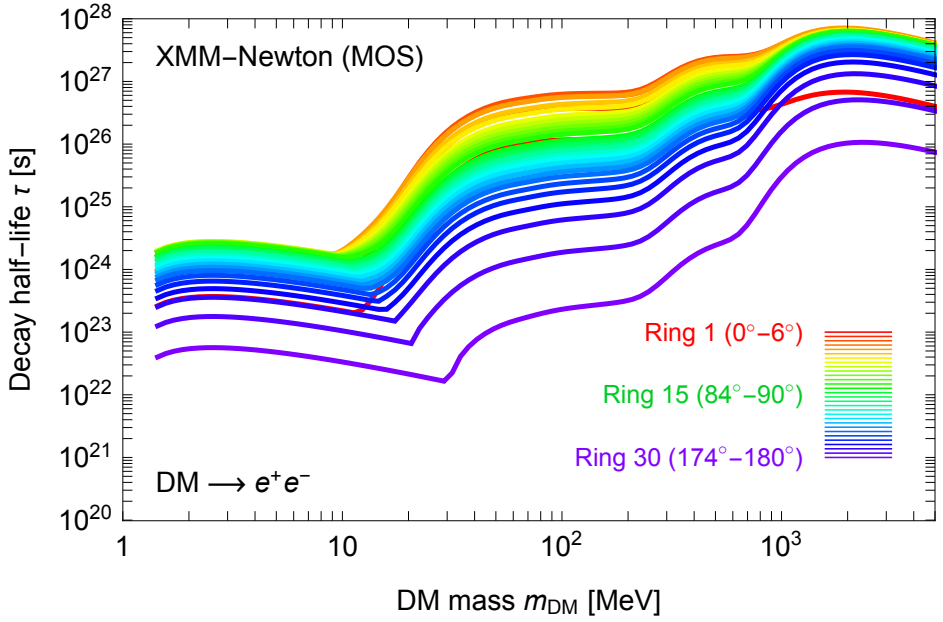

ICS halo function (spatial distribution)

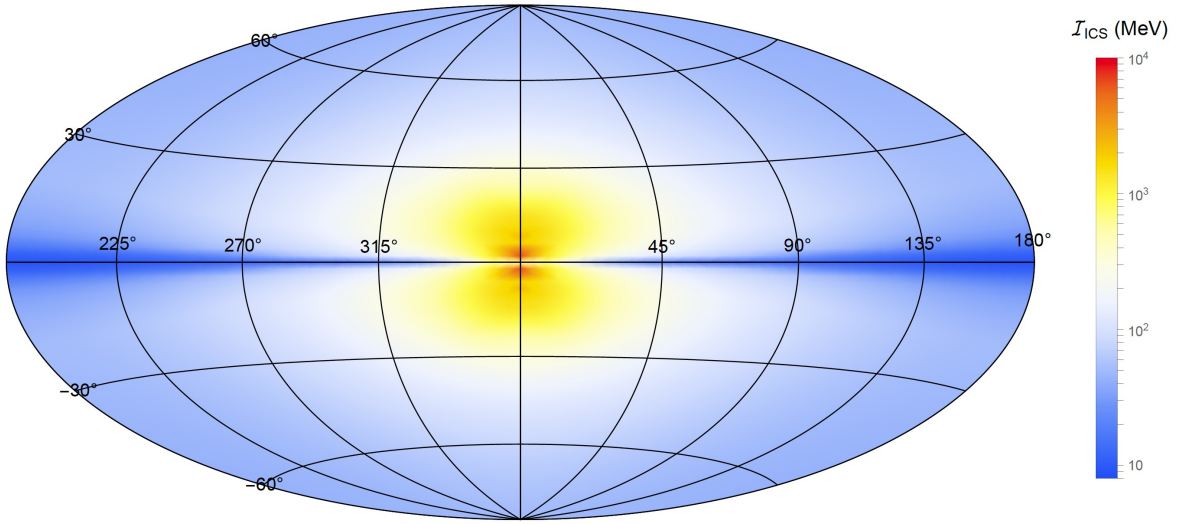

Annihilation ($\eta = 2$)

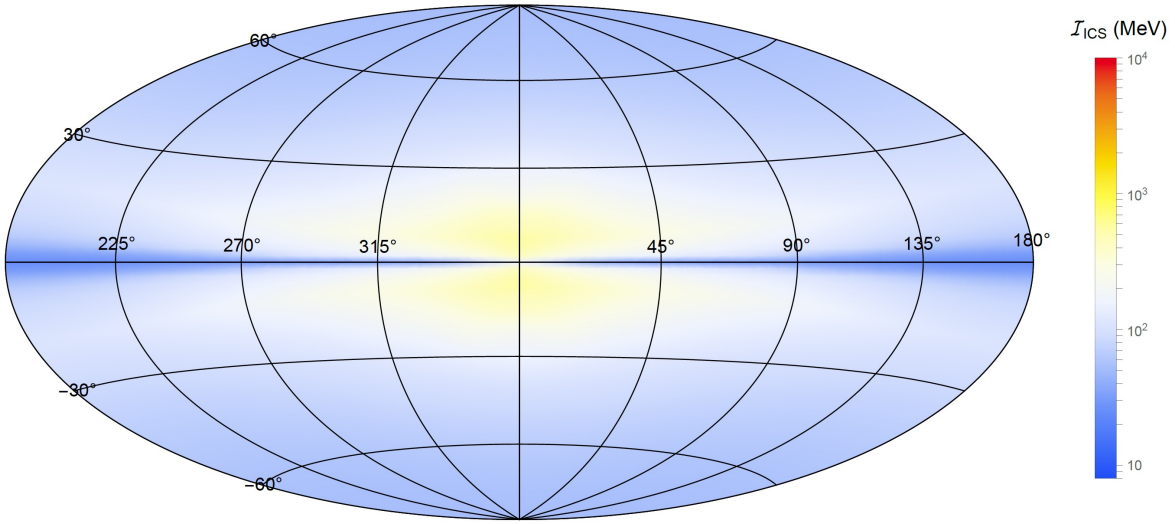

Decay ($\eta = 1$)

$$I_{ICS}(E_\gamma, E_e, b, l) = 2\, E_\gamma \int_{l.o.s.} \frac{ds}{r_\odot} \left(\frac{\rho(s,b,l)}{\rho_\odot}\right)^\eta \int_{m_e}^{E_e} dE\, \frac{\mathcal{P}_{IC}(E_\gamma, E, s, b, l)}{b(E, s, b, l)}$$

$E_\gamma = 5$ keV
$E_e = 1$ GeV

DM DM $\rightarrow e^+e^-$

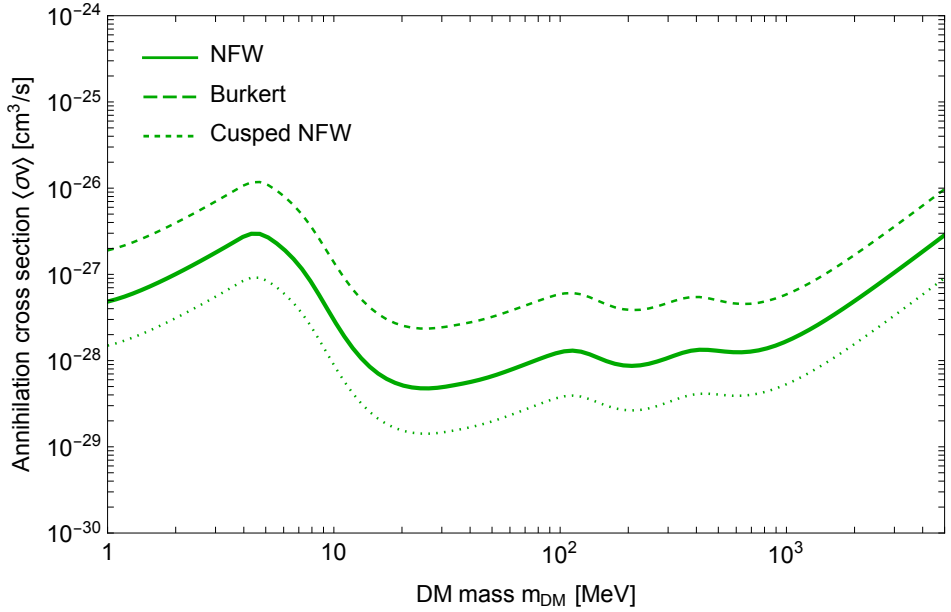

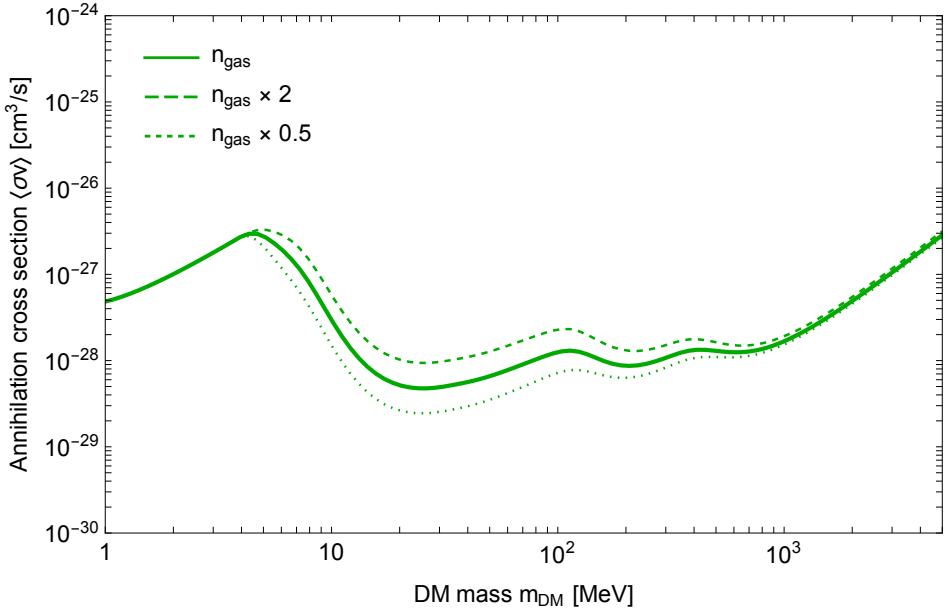

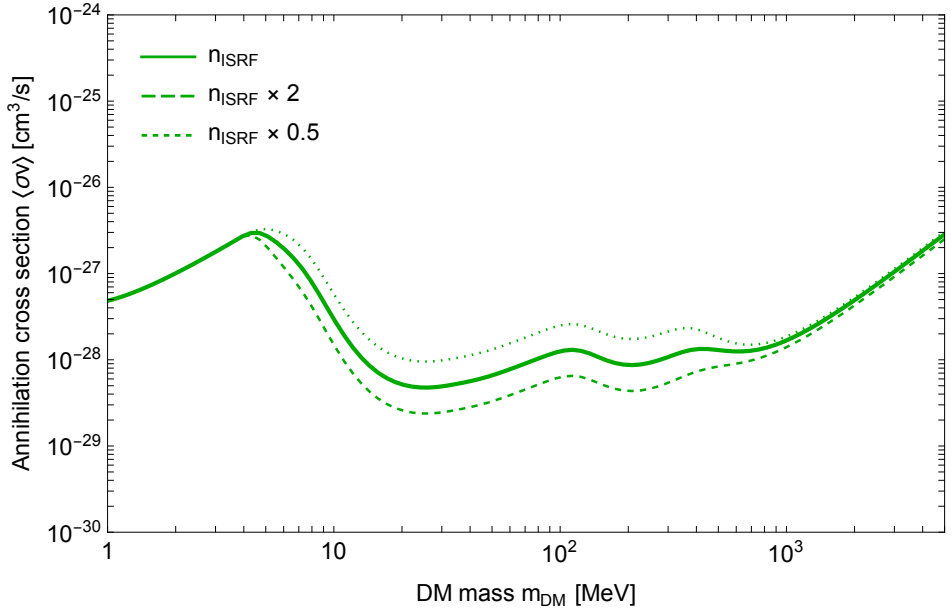

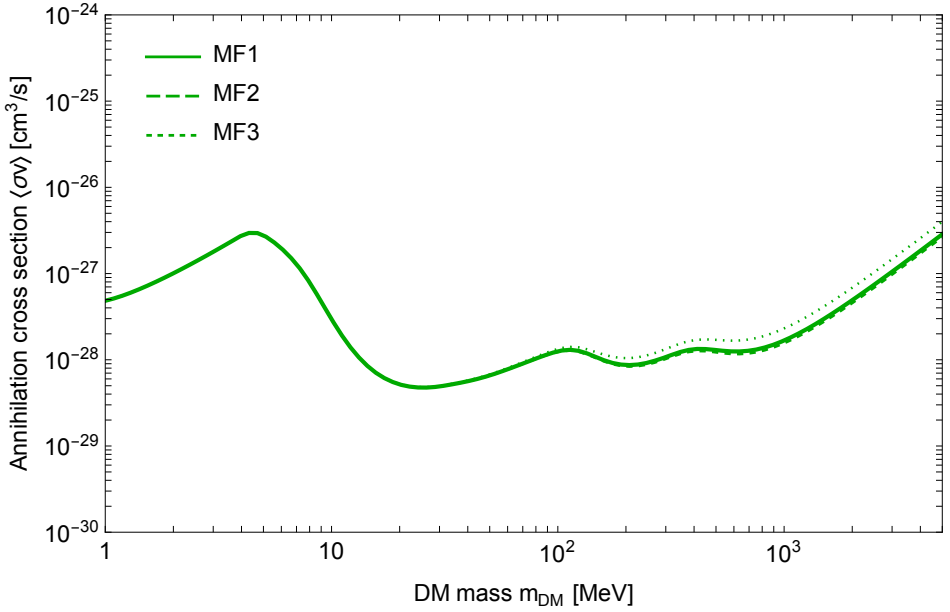

DM $\rightarrow e^+e^-$

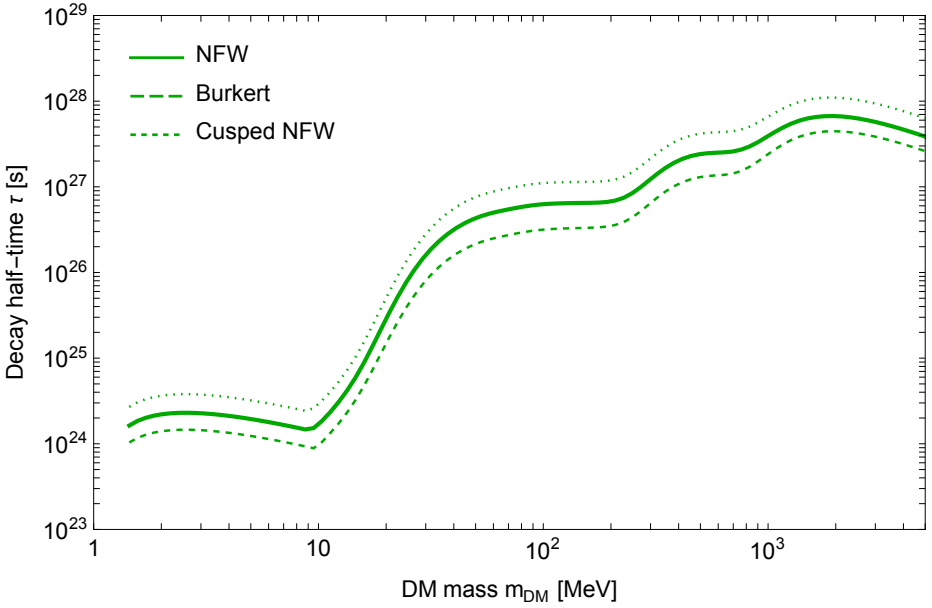

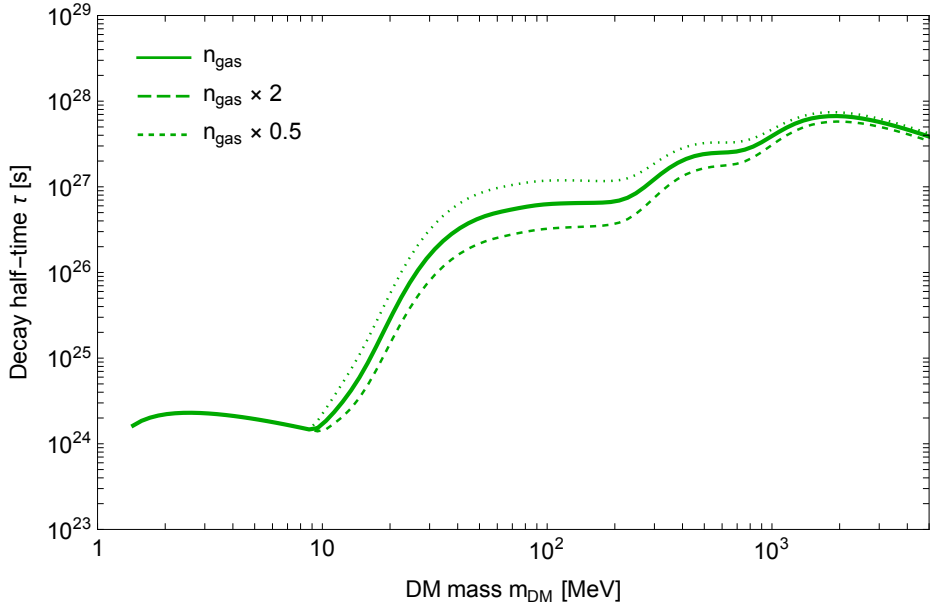

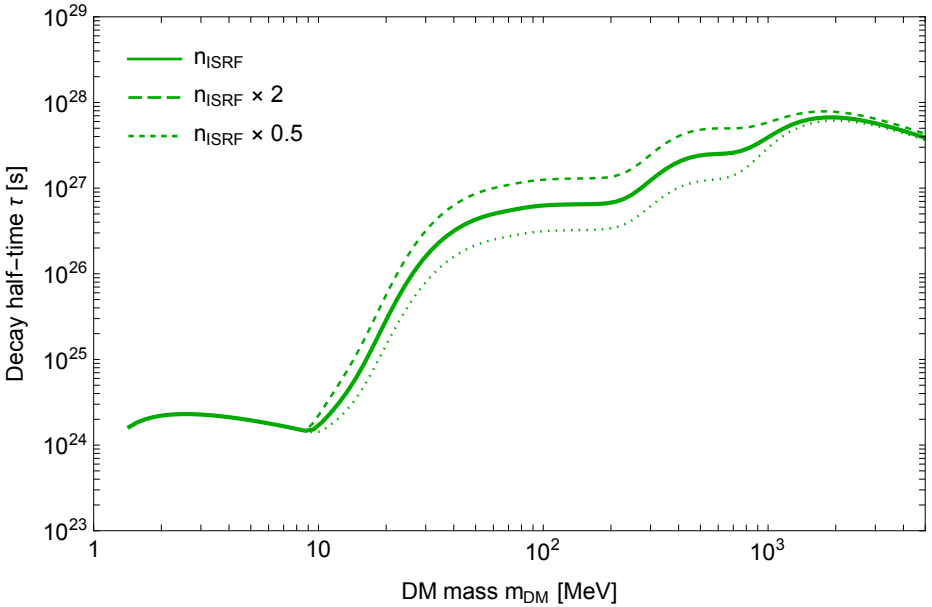

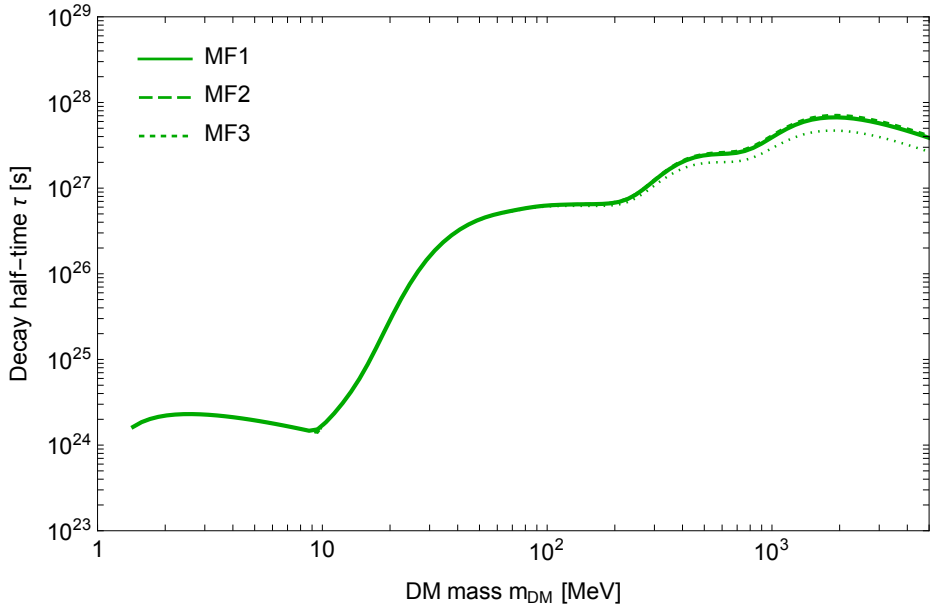

Galactic magnetic field configurations

$$B(r,z) = B_0 \exp\left(-\frac{r - r_\odot}{R_D} - \frac{|z|}{z_D}\right)$$

Models	$B_0\ (\mu G)$	$r_D\ (kpc)$	$z_D\ (kpc)$
MF1	4.78	10	2
MF2	5.1	8.5	1
MF3	9.1	30	4